A review of the pre-chamber ignition system applied on future low-carbon spark ignition engines

Sipeng Zhu[a], Sam Akehurst[b], Andrew Lewis[b], Hao Yuan[b*]

a School of Energy and Power Engineering, Shandong University, Jinan 250061, China.

b Department of Mechanical Engineering, University of Bath, Claverton Down, Bath BA2 7AY, UK.

* Corresponding author: Hao Yuan, E-mail address: hy310@bath.ac.uk.

Abstract

Legislations for greenhouse gas and pollutant emissions from light-duty vehicles are pushing the spark ignition engine to be cleaner and more efficient. As one of the promising solutions, enhancing the ignition energy shows great potential in simultaneously mitigating combustion knock and enabling lean-burn operation. Featured with distributed ignition sites, pre-chamber ignition systems with large or small pre-chamber volumes, auxiliary or no auxiliary fueling, and large or small orifices have gained a surge of interest in decreasing the fuel consumption and pollutant emissions.

This paper aims at presenting a comprehensive review of recent progress and development trends of pre-chamber ignition systems adopted on future low-carbon and low-emission spark ignition engines. First, mechanisms behind this technology are discussed from the perspectives of the pre-chamber scavenging and combustion, jet ejection, main chamber combustion, and emission formations. Second, the design criteria of pre-chamber geometries are presented in detail, followed by a discussion on the fuel and air management for the main chamber. Next, recent numerical and experimental studies on the pre-chamber ignition system and its applications in conjunction with other complementary technologies are summarized. Finally, critical issues for commercialization and future research directions are discussed.

Keywords:

Gasoline engine; Pre-chamber ignition; Turbulent jet; Passive and active configurations; Knock and lean combustion.

Nomenclature:

AFR	Air-fuel ratio
BMEP	Brake mean effective pressure
BSFC	Brake specific fuel consumption
CAD	Crank angle degree
CFD	Computational fluid dynamics
CI	Compression ignition
CO	Carbon monoxide
CO_2	Carbon dioxide
COV	Coefficient of variation
CR	Compression ratio
CSSR	Cold start spark retard
DI	Direct injection
DNS	Direct numerical simulation
EIVC	Early intake valve close
EGR	Exhaust gas recirculation
GDI	Gasoline direct injection
HC	Hydrocarbons
HCCI	Homogenous charge compression ignition
ICE	Internal combustion engine
IMEP	Indicated mean effective pressure
LES	Large eddy simulation
LIVC	Late intake valve close
MBF	Mass burn fraction
NO_x	Nitrogen oxides
ONR	Octane number requirement
PFI	Port fuel injection
PM	Particulate matter
PRF	Primary reference fuels
RANS	Reynolds-averaged Navier-Stokes equations
RCEM	Rapid compression expansion machine
RCM	Rapid compression machine
RPM	Rotation per minute
SCR	Selective catalytic reduction
SI	Spark ignition
SOI	Start of injection
TDC	Top dead center
TJI	Turbulent jet ignition
TKE	Turbulence kinetic energy

1 Introduction

1.1 Background and significance

The regulations for greenhouse gas and pollutant emissions are imposing more and more strength on the transportation sector. To achieve the long-term fleet target of 50 g CO_2/km for future automotive powertrains, the propulsion systems on light-duty vehicles are undergoing great changes from pure thermal engines towards more and more highly electrified powertrains [1]. Thus, the internal combustion engine (ICE) is still expected to be part of the powertrain in the following decades, and key technologies including further improving engine efficiency, advanced after-treatment systems, low carbon fuels, and predictive control strategies are being developed [2, 3].

Due to the restrictive emission regulations, spark ignition (SI) engines are becoming the dominant powerplants in the passenger car market. However, the SI engine with a lower compression ratio (CR) provides worse efficiency compared to its compression ignition (CI) counterpart [4]. Thus, further reducing fuel consumption from gasoline engines in future hybrid powertrains is now facing big challenges since peak efficiencies of larger than 45% have been repeatedly mentioned as target values [5-9].

1.2 Obstacles in low-carbon gasoline engines

The main obstacle in improving the thermal efficiency of the SI engine is the combustion knock. As an abnormal combustion phenomenon, knock significantly deteriorates the SI engine performance and reliability, especially for the downsized gasoline engine [10, 11]. Many methods of mitigating combustion knock have their own drawbacks, such as decreasing the engine thermodynamic efficiency, high cost, and unwanted side effects. Thus, knock is still commonly suppressed by retarding the spark timing and combustion phasing.

Another reason for the low thermal efficiency of the SI engine is the stoichiometric operation, compared to the lean-burn operation in the CI engine. The lean-burn concept, with the benefits of reduced heat losses through cylinder walls, increased specific heat ratio of the working fluid, and decreased pumping losses at part loads, is one of the most attractive solutions for reducing CO_2 emissions for the future hybrid gasoline engines [12-14]. However, the flame kernel growth and flame propagation are slowed down during the combustion process because of the reduced laminar flame speed of the lean mixture. This leads to a longer burning duration, incomplete combustion, and high cycle-to-cycle variations, which are detrimental to engine performance.

1.3 Methods to enhance the ignition

Enhancing the ignition energy with high-performance ignition systems is one good solution to simultaneously mitigate combustion knock and enable lean-burn operation with a relative air-fuel ratio (AFR) of 2 and above. Additional benefits of an enhanced ignition system include reducing ignition delay, allowing closer to TDC spark timing, and accommodating variations in charge motion and mixture homogeneity. Recent years have witnessed increasing research efforts on innovations of ignition technologies [15-17].

In general, ignition systems can be divided into two types, point ignition and space ignition [18]. The point ignition systems consist of single-spark ignition, multi-spark & dual coil ignition, and laser ignition. Concerning the space ignition, the ignition system itself ignites a larger share of the combustible volume. Compared to point ignition systems, space ignition systems like pre-chamber ignition, corona ignition, microwave ignition are characterized by higher ignition energy and reduced flame traveling distance [17, 19, 20]. Therefore, combustion benefits including the short combustion duration, improved combustion stability, and increased combustion efficiency are expected.

Yu et al. [21] categorized the primary ignition systems as the high-energy spark ignition, pulsed nanosecond discharge ignition, radio-frequency plasma ignition, laser-induced plasma ignition, and pre-chamber ignition. The ignition mechanisms, ignition effectiveness, and implementation challenges of those advanced ignition systems were reviewed in detail. In this work, pre-chamber ignition systems with distributed ignition sites are reviewed primarily. This ignition concept has been widely adopted on high power stationary powerplants [22-24] and is also known as the turbulent jet ignition

(TJI) in the frame of automotive applications [25].

1.4 History of the pre-chamber ignition system

Categorized with large or small pre-chamber volumes, auxiliary or no auxiliary fueling, and large or small orifices, the pre-chamber combustion system has a long history [25]. In the 1910s, the pre-chamber combustion system was first reported on a Ricardo Dolphin engine which relied on a passive auxiliary intake valve controlling fuel-rich mixture flowing into the pre-chamber cavity [26]. Inspired by this configuration, an additional fuel injector supplying the pre-chamber fuel was proposed in some designs, and the compound vortex-controlled combustion system from Honda could be the most successful example [19, 27, 28]. By removing the auxiliary pre-chamber fueling, some other engine concepts were proposed, including torch cell engines developed by manufacturers like Toyota [29], Ford [30], and Volkswagen [31]. Those early research works mainly focused on the pre-chamber combustion systems featured with large volumes. The large diameter throat connecting the pre-chamber and the main chamber enables continuous flame front propagation across those two chambers. However, the increased pre-chamber wall leads to larger heat transfer losses and higher hydrocarbon (HC) emissions. Hence, those large pre-chambers gradually disappeared in the past decades [25, 32].

The jet ignition is a subset of the pre-chamber combustion system, which was first introduced in the late 1950s by Nikolai Semenov and further developed by Lev Ivanovich Gussak [33, 34]. This concept is featured with a much smaller pre-chamber volume of 2~3% of the clearance volume, and the conventional single throat connecting the pre-chamber and the main chamber is replaced by a nozzle with multi orifices. A comprehensive review of early studies on different types of pre-chamber jet ignition systems including the ‘Jet plume injection and combustion’, ‘Hydrogen assisted jet ignition’, ‘Hydrogen flame jet ignition’, ‘Pulsed jet combustion’, ‘Swirl chamber spark plug’, and ‘Turbulent jet ignition’ was conducted by Toulson et al. [23]. The authors also noted that the TJI system proposed by MAHLE Powertrain is capable of operating with available commercial fuels like gasoline, propane, and natural gas, which overcomes hurdles of using hydrogen as the pre-chamber fuel in previous jet ignition systems. Thus, this review work will mainly focus on the more feasible TJI system rather than those laboratory-based jet ignition systems in early studies.

1.5 Influences of pre-chamber systems on combustion and emissions

The combustion initiated by the TJI system is quite different from the conventional SI combustion. The mixture in the pre-chamber is first ignited with a spark plug, and the pressure rise due to the flame propagation forces the hot products and active radicals to enter into the main chamber through the jet orifices. The high turbulence intensity and multiple ignition points provided by the turbulent jets promote the combustion in the main chamber. Thus, the TJI is an effective approach in accelerating combustion, improving combustion stability, and expanding the lean combustion limit on the SI engine.

Emissions generated in the cylinder are strongly dependent on the formation of the air-fuel mixtures, ignition, and combustion processes. Taking the direct-injected gasoline engine as an example, the increased hydrocarbons (HC), carbon monoxide (CO), and particulate matter (PM) are arisen from the short time for fuel evaporation and mixing. In a practical TJI case, the pre-chamber configuration, additional fuel injection, lambda level, and engine loads also play important roles in determining raw emissions. Thus, different variation trends of emissions were observed in the open literature. Nonetheless, the excess air and lower combustion temperatures with the lean-burn TJI system guarantee low HC, CO, and NO_x raw emissions.

Table 1 compares the conventional SI and CI systems with the novel TJI system from different combustion characteristics. The main combustion characteristics of the homogeneous charge compression ignition (HCCI) are also present. According to the comparative parameters, the TJI is superior to the conventional SI engine in fuel economy and pollutant emissions. With an auxiliary fuel injection system, the performance of the TJI engine can match that of the CI engine.

Table 1. Comparison of different combustion concepts in internal combustion engines [35-37].

	SI	CI	HCCI	TJI
Ignition	Spark ignition,	Auto ignition,	Auto ignition	Spark ignition

	single point	single point	multi-points	multi-points
Fuel injection	Gasoline like fuels, port or direct injection	Diesel like fuels, direct injection	Flexible fuels, and port or early direct injection	Flexible fuels in the pre-chamber if applicable
Air-fuel ratio	~1	1.2~2.2	2~8, depending on the fuel	Stoichiometric or lean
Flame	Turbulent flame propagation	Diffusion flame propagation	Homogeneous oxidation	Turbulent flame propagation
Major emissions	HC, CO and NO_x	NO_x and PM	HC and CO	Subject to design
Fuel economy	Good	Better	Best	Better

Due to the above unquestionable advantages and benefits, the pre-chamber combustion concept has gained a surge of interest in the past decades. This paper aims at presenting a comprehensive review of recent progress and development trends of pre-chamber ignition systems adopted on future low-carbon and low-emission SI engines. First, physical phenomena and mechanisms involved in the pre-chamber scavenging and combustion, jet ejection across the nozzle, and combustion and emission formations in the main chamber are discussed to provide insights into this technique. Second, the design criteria of the pre-chamber geometries, as well as fuel and air management in the main chamber are summarized. Next, current numerical and experimental activities on pre-chamber ignition systems with different implementations are reviewed. Finally, some critical issues arising from practical applications are presented.

2 Mechanisms behind the pre-chamber ignition system

The pre-chamber ignition systems discussed in this paper are categorized into two types, as illustrated in Fig. 1. The passive pre-chamber is filled during the compression stroke with homogeneous fuel-air mixtures available in the main chamber. The active pre-chamber system is integrated with an auxiliary fuel-metering device to accurately control the equivalence ratio of the stratified mixture. Thus, the passive pre-chamber system and the active pre-chamber system are also named the homogeneous pre-chamber system and the stratified pre-chamber system, respectively. Meanwhile, those two types share several distinct yet inherently related processes comprising mixture preparation and combustion inside the pre-chamber, jet formation and ejection across the nozzle, and flame initialization and development in the main chamber. The operating mechanism behind each physical phenomenon will be discussed in the following sections.

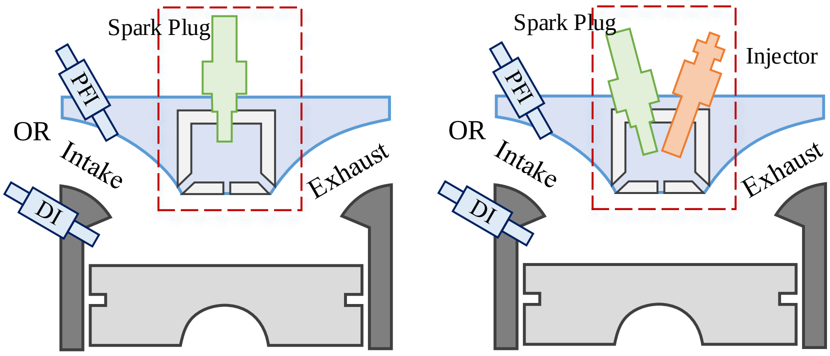

Figure 1. Configurations of passive (left) and active (right) pre-chamber ignition systems.

2.1 Scavenging and combustion in the pre-chamber

2.1.1 Pre-chamber scavenging

To maintain an inflammation zone around the spark plug gap and an overall stratified mixture that supports faster flame propagation within the highly turbulent pre-chamber, the scavenging and filling across the pre-chamber should be evaluated with special attention to the mass and energy transfer. The scavenging processes driven by pressure differences amongst intake/exhaust ports, pre-chamber, and main chamber can be divided into distinct phases according to the valve and piston movement [38, 39].

Blankmeister et al. [40] conducted a detailed CFD simulation to visualize the passive pre-chamber scavenging. The scavenging process during the intake stroke is illustrated in Fig. 2, and the pre-chamber is designed with nine orifice holes, hole diameters of 1 mm, and a centrally located spark plug. With the intake valve and piston moving down during the intake stroke, a small pressure difference between the intake side and the exhaust side is expected to drive the fresh charge scavenging across the nozzle orifices. This scavenging phase starts from the intake valve opening timing up to the point when the main chamber pressure exceeds that in the pre-chamber. During this period, a large amount of residual gas generated in the last cycle is still trapped inside the pre-chamber. Benajes et al. [41] indicated that the overall filling of the pre-chamber during the intake stroke is very small, which is normally less than 15%.

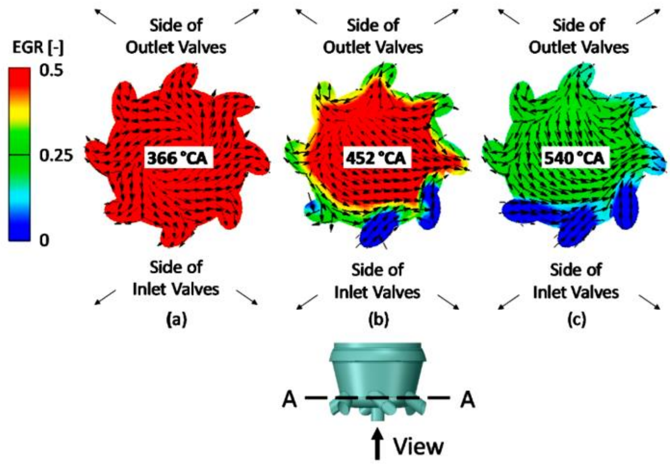

Figure 2. Scavenging across the pre-chamber during the intake stroke (EGR indicates the residual gas mass fraction) [40].

Indeed, the effective filling process normally starts during the compression stroke, and the mass transfer between the pre-chamber and the main chamber is mainly controlled by the piston moving. Benajes et al. [41] concluded that as long as a reasonable pre-chamber geometry is considered, the residual gas fraction level in the pre-chamber at the end of the compression is mainly determined by the CR rather than the pre-chamber geometric parameters like volume, nozzle length, and hole configurations. It should be noted that a reasonable pre-chamber design here mainly indicates selecting a reasonable value for the ratio of the total cross-sectional area of the holes to the pre-chamber volume since a too small area to volume ratio significantly deteriorates the scavenging efficiency and thus the following combustion process inside the pre-chamber.

Apart from the geometric CR, the residual gas fraction in the pre-chamber is also sensitive to the operating condition. This means the residual gas fraction normally increases at low load/speed and high load/speed conditions [41]. With respect to the active configuration, additional fuel injection could displace the residual gas and reduce the potentially negative impact of residual gas on pre-chamber combustion. Test results obtained by Bunce et al. [42] using a fast response CO_2 analyzer indicated that residual fraction inside the pre-chamber decreases when the fuel is injected directly. Moreover, the AFR in the vicinity of the spark plug can be controlled.

The turbulent kinetic energy (TKE) inside the pre-chamber should also be checked since the premixed combustion is strongly related to the turbulence field. Desantes et al. [43] indicated that the turbulence inside the pre-chamber is generated by the flow entering through the orifices and the additional fuel injection in the active configuration. Therefore, the pre-chamber geometry significantly determines the TKE and flow velocity. CFD results obtained by Almatrafi et al. [44] showed that high flow velocity is generated in the holes during the air-fuel mixture flows from the main combustion chamber into the pre-chamber. Thus, high TKE is generated in the upper region inside the pre-chamber during the inflow phase of the scavenging air flowing through orifice holes, which is occurred in the compression stroke. As shown in Fig. 3, Blankmeister et al. [40] plotted the correlations between the pre-chamber geometries and the TKE levels at 695 °CAD. CFD studies on different pre-chamber designs indicated that decreasing the volume or increasing the hole diameter increases the scavenging quality, but deteriorates the TKE. Meanwhile, the levels of TKE inside the pre-chamber are always lower than the main chamber level regardless of the pre-chamber geometric variants.

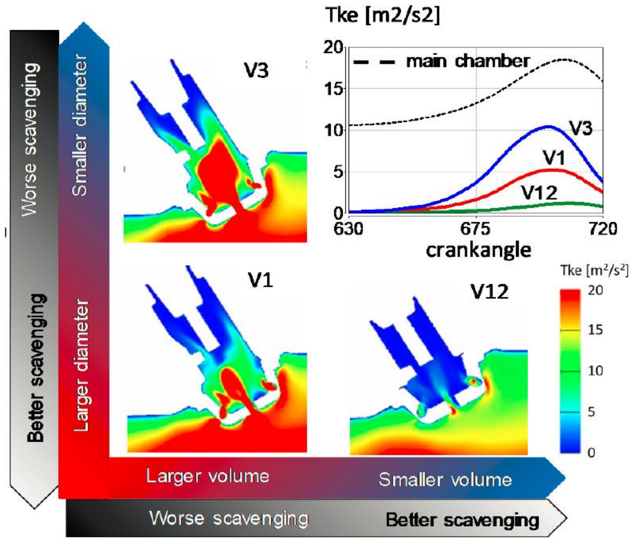

Figure 3. Correlations between the pre-chamber geometries and the TKE levels [40].

2.1.2 Pre-chamber ignition and combustion

Similar to the conventional SI engine, the mixture in the pre-chamber is ignited by a spark plug, followed by conventional premixed flame propagation. Since the flame dynamics in the main chamber is different from that in a conventional SI engine, the spark timing should be adjusted to accommodate the change.

Attard et al. [45] evaluated a modern gasoline SI engine with its pre-chamber filled with propane. The results indicated that IMEP is not sensitive to the change of spark timing under the experimental condition at 1500 rpm and λ of 1.8, while the optimum coefficient of variation concerning the IMEP is achieved with the spark timing around 26-27 °CA before TDC, which relies on the interactions between the pre-chamber and the main chamber. Liu et al. [46] studied the impact of the pre-chamber combustion on a single-cylinder SI engine fueled with kerosene under stoichiometric conditions. Test results suggested that the spark timing needs to be retarded after switching from dual spark plug ignition to pre-chamber jet ignition in order to control knock, which can be attributed to the increased temperature and pressure of the unburned gas mixture. Novella et al. [47] indicated that the pre-chamber geometry design limits the operating range of spark timing. Owing to the complexity of the pre-chamber system, the experimental findings are dependent on the geometry of the pre-chamber and the main chamber, as well as the fuel properties.

The laminar flame speed, which is mainly determined by the temperature, pressure, and mixture contents inside the pre-chamber, has significant effects on the flame structure and propagation velocity [48]. Evaluating on a single-cylinder gasoline engine with the compression ratio of 13.4:1, Novella et al. [49] indicated that it takes around 4 crank angle degrees (CAD) for the flame to sweep the entire pre-chamber volume and reach the bottoming orifices when the engine operates at 12.8 bar IMEP @ 4500 rpm. As illustrated in Fig. 4, Peters et al. [50] defined the pre-chamber combustion duration as the length of the pre-chamber pressure rising above that of the main chamber in units of crank angles. This is also indicated by the cross points of the main chamber and pre-chamber pressure traces.

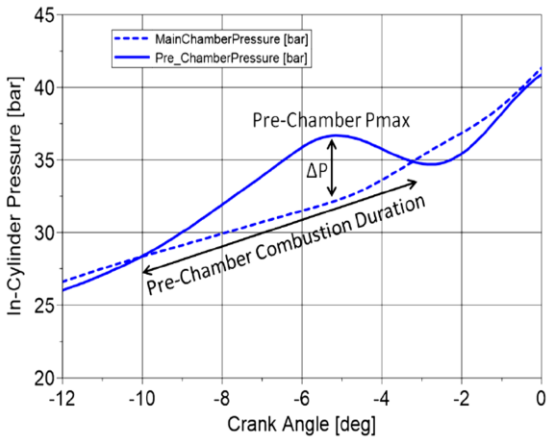

Figure 4. Pre-chamber combustion duration indicated by pressure traces in the pre-chamber and the main chamber [50].

It is worth mentioning that a flow reversal phase is normally observed after the main chamber charge is ignited. If the backflow from the main chamber to the pre-chamber contains fresh mixtures or intermediate combustion species, a second peak in the heat release process will occur inside the pre-chamber [51]. Distaso et al. [52, 53] also named this phenomenon as a “reburning phase”. However, this second heat release only accounts for a very small proportion of the total heat release inside the pre-chamber. Thus, the effects of the “reburning phase” on the jet ejection and the main chamber combustion are neglectable.

The pre-chamber combustion initiated by a spark plug is assumed to be similar to that of a conventional spark ignition engine. However, the small pre-chamber volume, the high surface-to-volume ratio, and the intense turbulence bring significant differences for the flame propagation in the pre-chamber [54]. With a small pre-chamber volume, the wall introduced quenching is much more critical since the flame develops near the wall, and the early kernel development phase occupies a large percentage of the overall pre-chamber combustion. The high surface-to-volume ratio of the pre-chamber increases the relative significance of heat transfer. The flame propagation is associated with turbulent intensity. However, the turbulence and stratification conditions inside the pre-chamber are not suitable for ignition and flame propagation compared to the conventional SI engine. Meanwhile, the flow laminarization close to the wall leads to a reduction of the flame speed.

Xu et al. [55] pointed out that the turbulent integral length is significantly suppressed by the small volume of the pre-chamber, compared to the main chamber combustion. The 3D CFD analysis based on the Borghi-Peters diagram indicated that the combustion events, for both the pre-chamber and main chamber, cover a wide range of turbulence intensity and length scales since changes in length scale ratio are far more significant than the changes in the velocity scale ratio. This further brings challenges for the simulation of the flame-turbulence interaction. Thus, Xu et al. [55] proposed a blending function to account for the large- and small-scale turbulence in modeling the turbulent flame speed. Xu et al. [55, 56] also testified that the G-equation based on Reynolds-averaged Navier-Stokes equations (RANS) integrated with two specific sub-models is capable of predicting the global combustion phenomenon, like the heat release and mean flame front propagation.

2.2 Jet ejection and ignition

2.2.1 Jet ejection

After the pre-chamber combustion, the pressure difference arising from the combustion in the pre-chamber drives the flame and partially oxidized species into the main chamber. With a small ratio of the orifice hole area to the pre-chamber volume (~0.03 cm^{-1} in some cases), the flame is quenched in the long orifice channel [18]. To visualize the jet ejection process, Chinnathambi et al. [57] conducted detailed CFD simulations. In general, the jet ejection from the pre-chamber into the main chamber can be divided into three phases, according to variations of the temperature and the mass fraction of the intermediate reaction products [52]. The first stage is the cold jet phase with the unburned mixture exiting the pre-chamber, due to the spatial position of the spark electrodes [38, 39]. This also leads to a retarded ignition in the main chamber. In the second phase, the high-temperature intermediate reaction products eject from the pre-chamber and then ignite the mixture in the main chamber. The third phase is characterized by a significantly decreased temperature of the ejected mixture with low values of the mass fractions of the intermediate reaction products. This indicates that the rich part of the mixture in the pre-chamber is eventually ejected.

Pressure traces and high-speed images obtained from the optical engine could also provide fundamental insights into the jet ejection process. Optical diagnostics on a single-cylinder natural gas engine performed by Rajasegar et al. [58] indicated that the driving force that governs the formation, development, and mixing of the turbulent jets in the main chamber is almost determined by the air-fuel ratio in the pre-chamber, regardless of the varying air-fuel ratio in the main chamber. By adopting the negative acetone PLIF and OH* chemiluminescence imaging techniques on an optical engine, Tang et al. [59] testified that the jet penetration speed is closely related to the pressure difference between the pre-chamber and main chamber. Bunce et al. [60] performed comprehensive optical research on the jet ejection process as well. As shown in Fig. 5, the visible jets or burned products first appear in the main chamber at 9 CAD before the top dead center (TDC). The obvious disparity between the pre-chamber and main chamber pressure traces from -13 to -10 CAD after TDC indicates that no reactive jet of unburned charge is forced into the main chamber. Further looking at the optical images, reactive and luminous jets appear in the main chamber but quickly dissipate due to the sudden drop in pressure and temperature encountered in the main chamber and the entrainment of fresh charge. Finally, distinctly distributed ignition sites appear in the main chamber from 5 CAD before TDC.

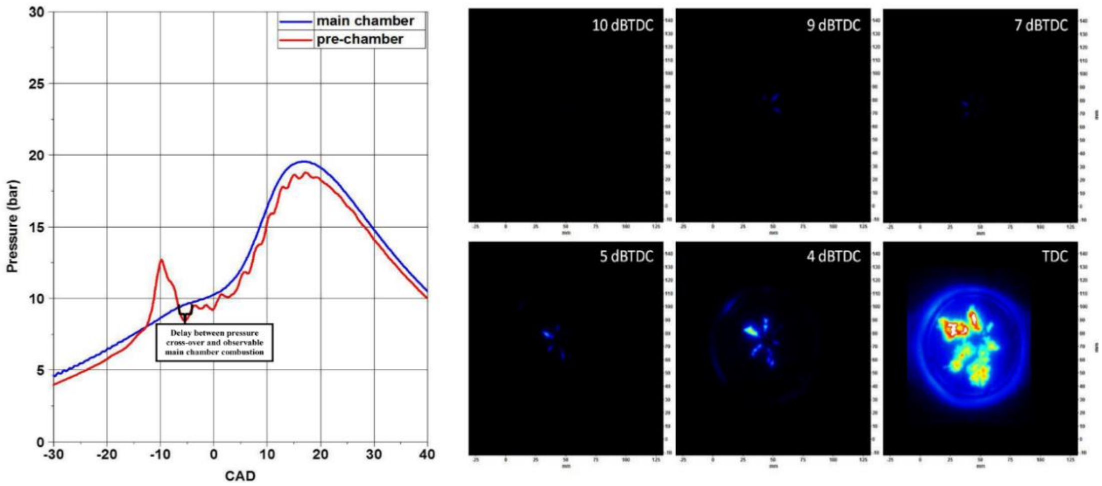

Figure 5. Pressure traces (left) and visualizations (right) during jet ejection processes on an optical engine [60].

The jet penetration prior to ignition determines the distributions of ignition sites. Bunce et al. [60] indicated that jet penetration shows a strong correlation with jet velocity. A lower jet velocity results in a lower level of penetration and longer combustion duration. On the contrary, a high jet velocity leads to penetration further away from the nozzle center. This could also lead to fewer ignition sites due to wall quenching. Meanwhile, the jet velocity also has a big influence on the turbulence level for the main chamber combustion. Thus, the jet velocity should be targeted in the pre-chamber design to maximize ignition site distribution while preventing jets from traveling to walls and quenching.

2.2.2 Jet ignition

As exemplified by the Ricardo Dolphin and Honda 'compound vortex-controlled combustion' designed with large diameter throats, the flame ignition or named torch ignition can promote flame propagation between those two chambers [25]. Replacing the large diameter throat with a nozzle comprising small orifices, the pre-chamber flame front is quenched as the products exit through the orifice channel. Thus, the flame quenching caused by limiting the diameter of the orifices in the nozzle differs the TJI from the traditional torch-ignition system.

Biswas et al. [61, 62] conducted experimental studies on the TJI characteristics of CH_4/air and H_2/air mixtures in a generic single-hole pre-chamber adopted on a combustion bomb. The ratio of the main chamber volume to the pre-chamber volume was fixed at 100, and a stainless-steel orifice plate with a diameter ranging from 1.5 to 4.5 mm separated both chambers. The initial pressure changes from 0.1 to 0.5 MPa in the tests. With the help of simultaneous high-speed Schlieren and OH* chemiluminescence imaging, experimental results confirmed two distinct ignition patterns according to the ignition delay in the main chamber and the flame morphology: the jet ignition with hot jets comprising only combustion products and the flame ignition with hot jets containing wrinkled turbulent flames and active radicals. Since an increased flame thickness is expected with the decreased temperature and pressure, Biswas et al. [62] also concluded that the ignition mechanism shifts from jet ignition regime to flame ignition with the increase of the chamber pressure and orifice diameter.

Yamaguchi et al. [63] studied mechanisms behind the torch jet ignition using a divided chamber bomb. The effects of the nozzle diameter and chamber volume ratio on the structure of the torch jet were examined under both uniform and stratified conditions. Based on the optical results, four patterns of ignition in the main chamber were observed, including the chemical chain ignition, composite ignition, flame kernel torch ignition, and flame front torch ignition. Wöbke et al. [64] carried out optical studies on a combustion vessel with methane/air mixtures. Measurements of simultaneous Schlieren and OH* chemiluminescence identified three different mechanisms inside the main chamber, which include ignition by a reacted jet, ignition by a reacting jet, and a combination of both. Experimental work conducted by Gussak et al. [65, 66] concluded that jets containing hot but complete combustion products generated with the stoichiometric or slightly leaner mixture inside the pre-chamber have much lower reactivity compared to the jets containing a large number of reactive radicals generated by burning a richer mixture.

As depicted in Fig. 6, Kyrtatos et al. [67] indicated there are two distinct mechanisms accounting for the quenching in a turbulent reacting jet passing through a nozzle. The thermal quenching is mainly driven by the heat loss from the flame to the surrounding walls, especially when the flame approaches the orifice [68]. With the heat loss exceeding the heat release of the flame, the reduced temperature prevents chain-branching reactions from being sustainable, and only radical recombination reactions can take place. With a larger flame thickness and a narrower nozzle, thermal quenching is more likely to happen. Another mechanism is the hydrodynamic quenching, which arises from the intense mixing of combustion products from the pre-chamber with the cold unburned mixture in the main chamber. However, the increased hydrodynamic quenching might lead to the global quenching of the flame in extreme conditions, like the low temperature and unsuitable air-fuel ratio conditions. Those conditions are unfavorable for flame kernel development and flame propagation, which lead to misfiring in the main chamber.

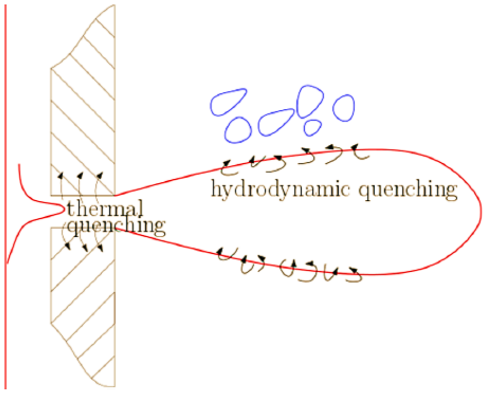

Figure 6. Schematic of different quenching mechanisms in the turbulent jet ignition [67].

Flame quenching has also been observed in some CFD studies. To visualize the quenching phenomenon, Chinnathambi et al. [57] plotted the iso-temperature contours of jets flowing across the nozzle on a two-dimensional mid-plane. The result showed that the hotter temperature regions of 2400 K within the pre-chamber could not penetrate into the main chamber in the crank angle range of -10 to -9 CAD before TDC. Thus, high-temperature boundaries are confined within the pre-chamber while main chamber reactions proceed at lower temperatures.

To provide fundamental insights into jet ignition, Bunce et al. [60] performed detailed optical studies on a retrofitted metal engine. The OH* and CH* intensities at 2 CAD after the first appearance of visible jets indicated that jets only contain little if any detectable CH*. This means the nozzle orifices effectively quench the flame front.

2.3 Combustion in the main chamber

2.3.1 Ignition and flame development

The high-temperature turbulent jets containing chemically reactive radicals (O, H, and OH) ignite the mixture in the main chamber with chemical, thermal and turbulent effects, which dominate the whole combustion process in the main chamber. The chemical effect refers to the radicals present in the jet which are highly reactive. Those partially or fully burned combustion products in jets are at high temperatures and could be potential thermal triggers in the main chamber. A high jet velocity means a long penetration distance, and more air-fuel mixture could be entrained in the main chamber. This is also named the turbulent effect. Compared to that of the conventional spark plug, the pre-chamber ignition system with multiple ignition sources could amplify the ignition energy by more than two orders of magnitude [53].

Muller [69] conducted detailed RANS and large eddy simulation (LES) of a rapid compression machine (RCM) to figure out the inherent combustion mechanisms in the main chamber. To isolate the thermal and chemical effects induced by the hot jets on the main combustion, an inert case and a reactive case were simulated. In the inert case, all the active radicals in the turbulent jet were replaced by CO_2, H_2O, and N_2. Thus, the turbulent jet is non-combustible. For the reactive case, all the radicals in the GRI_Mech 3.0 mechanism are included. Therefore, both the thermal and chemical kinetic effects on the ignition process are studied. The result showed that the ignition in the main chamber is faster in the reactive case compared to the inert case. This means the chemical kinetic effects are important for the ignition in the main chamber.

Using a zero-dimensional pre-chamber combustion model developed based on the CHEMKIN-PRO software, Tang and Sarathy [70] conducted a thorough investigation of the chemical effects of the turbulent jet on the main chamber ignition. Simulation results of varied equivalence ratios of reactants suggested that burning around stoichiometric conditions can generate more reactive radicals especially H and OH radicals and thus promote the ignition performance of the ultra-lean mixture in the main chamber. The heat release rate and laminar flame speed are likely to be promoted with more low-carbon species from the pre-chamber burning with a relatively rich mixture. By adopting DNS with detailed chemical kinetics, Qin et al. [71] investigated the ignition mechanisms in a simplified pre-chamber/main-chamber system burning with methane/air mixtures. It was found that the heat release rate is approximately proportional to the mass fractions of CH_2 and OH. This indicates that the chemical effect has significant effects on flame stabilization and propagation.

Further looking into the combustion process in the main chamber, it first occurs inside the hot jets at multiple locations. After the whole entrained mass inside the hot jets has burned rapidly, the flame reaches the jet boundaries and then progresses outside the jets as a well-established flame front. Thus, the turbulent effect mainly determines the flame propagation inside the main chamber. As illustrated in Fig. 7, Novella et al.

[41, 49] compared the main chamber combustion processes under the stoichiometric condition and the lean burn condition. The results indicated that under the stoichiometric condition, the fuel mass entrained by the turbulent jets is ignited and consumed first. Since the flame reaches the jet boundaries in a short time and the thermodynamic and turbulence conditions outside the jets are favorable for flame propagation, only a small amount (less than 15%) of the energy is released inside the jets. With respect to the ultra-lean burn case, the thermo-chemical and turbulence condition outside the jet boundaries hinder the flame propagation. Thus, most of the fuel energy (more than 90%) is still released outside the jets, and the amount of energy released inside the jets is relatively low compared to that in the stoichiometric case.

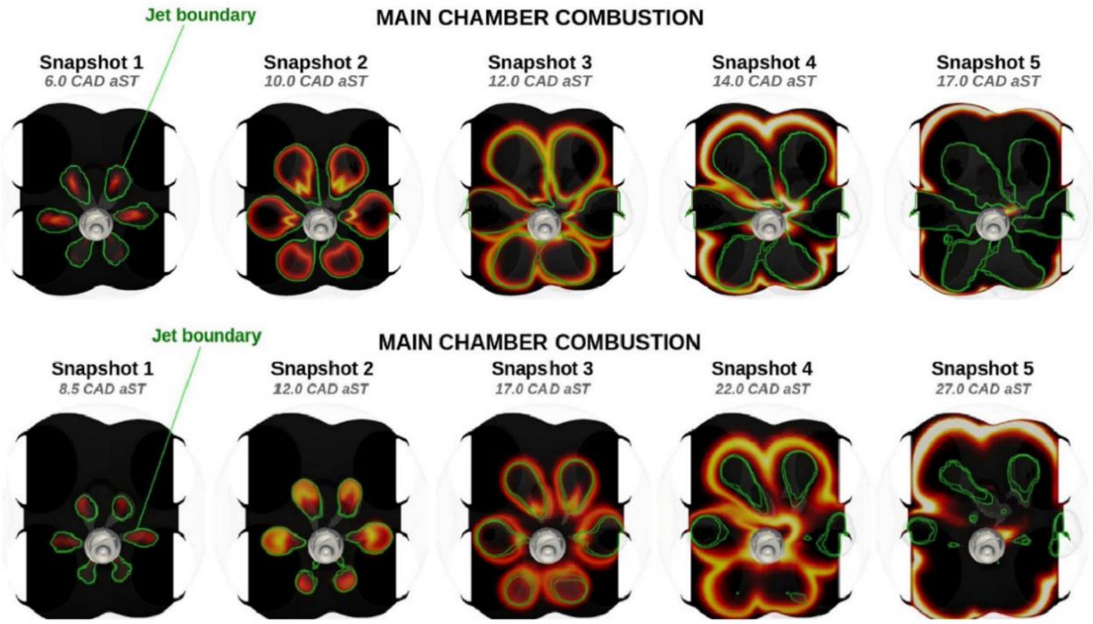

Figure 7. Visualization of the main chamber combustion at (top row) stoichiometric conditions and (bottom row) diluted conditions [49].

Experimental studies based on optical measurements reveal details of the in-cylinder combustion process. Korb et al. [72] conducted optical measurements of averaged flame probability distribution in a natural gas engine, and the investigated cases consisted of two nozzle orientations (A: radical, B: tilted), two different equivalence ratios in the main chamber (λ), and two different fuel flows in the pre-chamber (m_f), they were compared at a sequence of crank angles, as shown in Fig. 8. In A-11, turbulent jets emerge from the nozzles of the pre-chamber and start to grow in both longitudinal and lateral directions owing to the turbulent flame propagation. The comparison between A-11 and A-21 suggests that a leaner mixture impairs the combustion process, as the jets are partially extinguished (from -5 to -3 °CA in A-21) which slows down the combustion. With more fuel added in the pre-chamber in A-22, turbulent jets emerge earlier than both A-11 and A-21, leading to an increased combustion rate compared with that of A-21, which, however, is not sufficient to compensate for the negative impact from a leaner mixture on the combustion rate. Compared with the measurements of A-21, the tilted nozzles in B-21 result in lower jet penetration speed due to reduced turbulence, which, consequently, slows down the combustion in the main chamber. Nevertheless, the combustion stability is improved by the tilted nozzles, since the slow jets have small flame stretch and low dilution rate, which results in a short ignition delay and a high ignition probability. Based on a pre-chamber engine fueled with methane, an optical study conducted by Tang et al. [59] found that over-enrichment in the pre-chamber reduces the jet penetration velocity. Meanwhile, details on a post jet discharge process were provided, like two unburned regions in the main chamber and the change of reaction zone with the jet penetration.

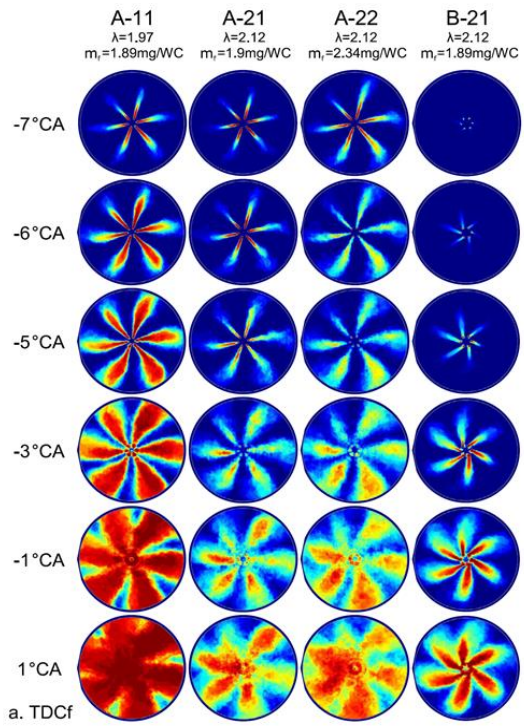

Figure 8. Comparison of averaged flame probability distributions in four cases [72].

2.3.2 Heat release rate

In practical applications, it is common to use mass burn fraction (MBF) to represent the percentage of energy release from the fuel. The start of combustion is generally considered as 0 to 10% MBF. Based on the measurement on a rapid compression machine (RCM) with a pre-chamber, Gentz et al. [73] suggested that the burn duration of the start of combustion with TJI is generally shorter than those from a baseline SI engine, especially with relatively small nozzle sizes. Similar trends were observed in Refs. [42, 46, 74, 75].

Despite the pre-chamber ignition retarding the combustion start phasing, its distributed ignition sites and increased jet turbulence enable fast and intense combustion. Bunce et al. [42] compared combustion events of a passive TJI system and a conventional central spark plug at an engine BMEP of 18 bar @ 4000 rpm. As illustrated in Fig. 9, there exists a spike in the pre-chamber pressure trace prior to the firing TDC. This initiates rapid combustion in the main chamber, which is illustrated by the integrated heat release curves shown in Fig. 9. The combustion duration of mass burn fraction (MBF) 10-90 could be reduced by 40% using passive TJI, and the center of the combustion phasing is advanced by 9 CAD. Therefore, high in-cylinder peak pressure and rapid pressure rise are always expected with the TJI.

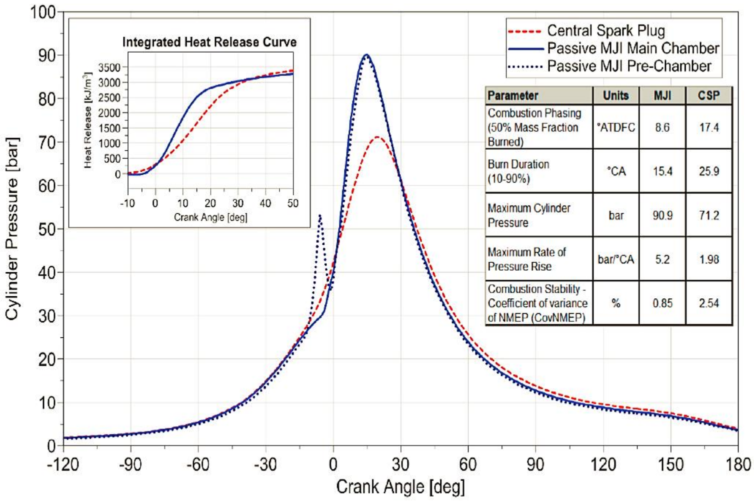

Figure 9. Comparison of the combustion profile between the passive TJI and the conventional SI at BMEP of 18 bar @ 4000 rpm [42].

The heat release curve in the main chamber could also provide distinct combustion information of the TJI engine [76]. The early combustion phase of MBF 0-10 encompasses information of the pre-chamber combustion, jet ejection, and main chamber ignition. This combustion phase is significantly influenced by parameters like pre-chamber geometry, scavenging, auxiliary fueling, and spark timing. The following combustion phase of MBF 10-50 is mainly referred to as the combustion process after jet ignition and therefore is still mainly influenced by the jet characteristics, like the jet-induced turbulence level and the entrainment of the surrounding fresh charge. The later combustion phase of MBF 50-90 is dominated by the flame propagation in the main chamber.

Further looking into the physical principle of the main chamber pressure traces, the jet ejection from the pre-chamber creates a strong pressure wave propagating into the main chamber. This initial disturbance generated at the beginning of the overall combustion is then amplified by the increasing main chamber pressure. Therefore, the amplitude of the pressure oscillation in the TJI is higher compared to the conventional SI engine [75]. As shown in Fig. 10, Sens et al. [75] compared filtered cylinder pressure traces with the conventional spark plug ignition and the pre-chamber ignition. The authors also indicated that the pre-chamber geometries that determine the excess pressure built up inside the pre-chamber also have significant influences on the pressure oscillation in the main chamber. Hua et al. [77, 78] also indicated that the pressure oscillations in TJI combustion arise from the local fast burning rate of the hot jets, which are different from the pressure oscillations in the SI engine caused by end-gas auto-ignition.

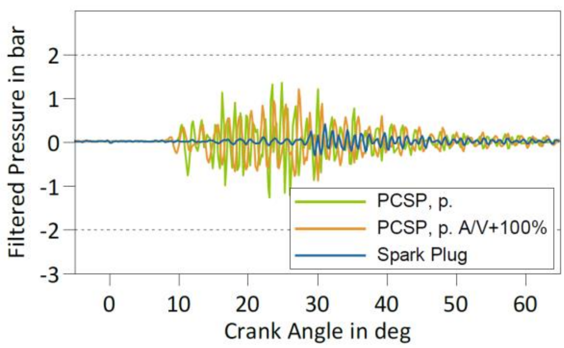

Figure 10. Comparison of filtered pressure traces between the conventional spark ignition and the pre-chamber ignition at BMEP of 16 bar @ 2000 rpm [75].

2.3.3 Knock suppression

As has been discussed, the pre-chamber ignition system is supposed to increase the combustion rate in the main chamber by enhancing the in-cylinder turbulence and generating multiple ignition sites. The reduced burn duration, normally by 30~50% compared to that of the conventional SI engine, means shorter end gas residence time. Also, the mixture in the main chamber is burned from the outer areas of the chamber to the middle areas with the pre-chamber ignition system, compared to the conventional flame propagating from the central spark in a conventional SI engine. This means the flame reaches the areas normally suffering from combustion knock much earlier, such as the piston top ring. Thus, knocking combustion can be mitigated. This allows exploiting the thermal efficiency with other approaches.

To compare knock limits of passive TJI and conventional SI systems, Attard et al. [79] performed experiments of seven PRF (primary reference fuels) blends ranging from 60 to 93 octane number in a stoichiometric single-cylinder engine operating at 1500 rpm and wide-open throttle conditions. Test results showed that the passive TJI system leads to an improvement of 10 octane number requirement (ONR) over the conventional SI system at the maximum brake torque combustion phasing. Meanwhile, the passive TJI system is capable of operating on 65 octane fuel at the limit of combustion stability. The active pre-chamber ignition system featured with a slightly rich pre-chamber mixture enables a further 3 ONR improvement at the same maximum spark retard. This mainly results from the improved jet reactivity and penetration and hence less jet variability from cycle to cycle.

It is worth noting that the passive TJI system is more likely to be adopted to take the advantage of the knock limit extension, considering the hardware design and cost. Cooper et al. [74] conducted experimental studies on the passive TJI for knock mitigation over a load sweep from 6 bar up to 18 bar BMEP, and key findings are illustrated in Fig. 11. In the conventional SI engine, the knock limited engine performance occurs at the BMEP of 12 bar. At higher engine loads, the combustion phasing is retarded to avoid knock which increases the MBF 10-90 and reduces the combustion stability. The optimum combustion phasing with TJI increases the BMEP to 16 bar, and combustion phasing is improved by 8 to 9 CAD for this application. The fast combustion duration and improved combustion stability are observed over the whole load range. One negative effect of faster burn rates with jet ignition is the increased pressure rise rates. The maximum rate of pressure rise is significantly increased over 5 bar per crank angle degree which is at the upper limit for a production engine to avoid combustion noise and maintain the desired NVH characteristics of the vehicle. The improved combustion characteristics could only translate into a brake specific fuel consumption (BSFC) benefit at the highest loads, due to the significantly improved combustion phasing. The fuel economy starts to deteriorate when the load drops below the BMEP of 14 bar. This is mainly due to the higher thermal loss from the non-optimized pre-chamber. To compensate for this thermal loss and increase the engine efficiency at low loads, increasing the geometric compression ratio is suggested.

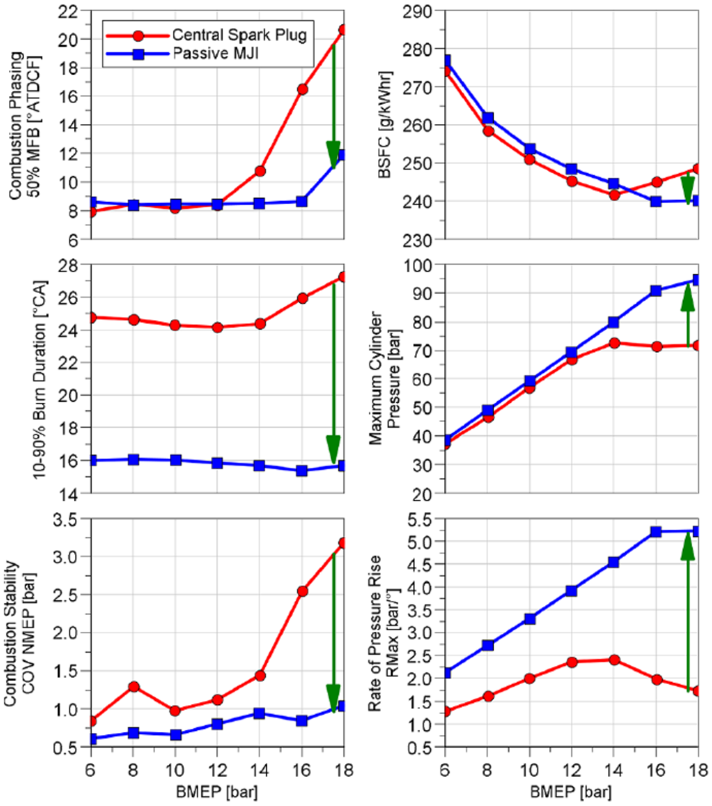

Figure 11. Comparison of the passive TJI and the conventional SI over a BMEP sweep from 6 bar up to 18 bar at 4000 rpm [74].

2.4 Emissions

2.4.1 Emissions in passive pre-chamber engines

Pollutant emissions from the gasoline engine are CO, HC, NO_x, and PM. Raw emissions in the exhaust gas largely depend on fuel and air management. Due to the short time for fuel evaporation and mixture formation as well as the fuel impingement on cylinder walls, the GDI technology is featured with increased HC, CO, and PM. PM emissions from spark-ignited engines are not an issue with the port fuel injection (PFI) system providing excellent mixture homogeneity [80].

Emissions from a TJI engine are determined by lots of factors like the pre-chamber configuration, additional fuel injection, lambda, and engine loads [81]. Concerning the operation of the passive pre-chamber engine, there is no auxiliary fuel injection, and the lean burn limit is comparable to that of the conventional gasoline engine. Thus, the pre-chamber design and fuel management for the main chamber largely determine the raw emissions from the passive pre-chamber engine.

Aiming at evaluating raw emissions from the passive TJI engine, Stadler et al. [33] evaluated four different orifice cap configurations with varied nozzle diameter, number of nozzles, and nozzle swirl angle. Compared to the conventional SI engine, the passive TJI is featured with overall lower CO and HC emissions, which indicates more complete combustion. The more intense combustion with the passive pre-chamber leads to increase combustion temperatures and thus increased NO_x emissions. With advanced combustion phasing and increased combustion temperatures, the pre-chamber ignition is supposed to improve the oxidation of the soot at higher engine loads. Meanwhile, the authors concluded that there is no clear tendency or significant difference in emissions among different pre-chamber configurations when the engine is tuned to maximize the thermal efficiency.

2.4.2 Emissions in active pre-chamber engines

Concerning the operation of the active pre-chamber system, the lean-burn concept is normally adopted, which plays a significant role in determining raw emissions. Thus, the CO emissions are expected to decrease at the beginning of the near-lean region, and the total HC emissions first drop in the near-lean region and then slowly increase in the ultra-lean region. The NO_x emissions first increase and then significantly decrease with the increasing lambda level. Particulates generated in the rich zones and inhomogeneous mixture in the pre-chamber could not be oxidized in the main chamber due to the low temperature at high lambda. Thus, a negative effect on particulate emissions is raised from the ultra-lean burn and charge stratification with separated pre-chamber and main chamber fueling [44]. In addition, the fuel injector might not be able to control the fuel mass in a small range at low loads, and increased particulate emissions could be excepted.

Experimental studies on NO_x emissions from an active TJI engine operating in the speed range of 1500~4000 rpm and at BMEP ranging from 2 to 11 bar were conducted by Attard et al. [82]. The results indicated that the percentage magnitude of NO_x reductions with increased lambda level is nearly independent of engine speed or load, and the engine-out NO_x reduction of 95%+ at ultra-lean conditions is expected. Stadler et al. [33] indicated that NO_x emissions can be reduced to 0.2 g/kWh with the ultra-lean operation of lambda up to 2. It is noted that the remaining NO_x emissions (<40 ppm) are assumed to be mainly generated in the pre-chamber combustion, as has been established in heavy-duty pre-chamber research.

Stadler et al. [33] evaluated the effects of the pre-chamber fuel mass flow ratio ranging from 0 to 8% on engine emissions. It is concluded that a too large pre-chamber fuel mass flow ratio leads to rich mixtures in the pre-chamber and contributes to the formation of soot. Atis et al. [83] suggested that compared to the excess air dilution, the EGR dilution is more effective in NO_x emission reduction but has a higher HC emission due to lower combustion efficiency. Beyond the lean-burn limit, the HC emissions increased more rapidly due to poor combustion stability and partial burning. An optical engine test conducted by Sementa et al. [84] indicated that the higher HC emissions with the active pre-chamber engine operating under lean conditions are attributed to the non-uniform behavior of turbulent jets from different pre-chamber orifices.

Based on a single-cylinder engine, Stadler et al. [33] compared emissions from different ignition systems at varied loads. As illustrated in Fig. 12, the passive pre-chamber configuration is featured with higher NO_x emissions compared to the conventional SI engine due to the intensified combustion leading to higher combustion temperature. The CO emission is generally lower with the active pre-chamber due to more complete combustion. The particulate emissions are relatively higher with the pre-chamber at low loads. While at high loads, an advanced spark timing leads to a longer period for the oxidation of the soot. In addition, the increased combustion temperature is supposed to improve soot oxidation. Lower HC emissions are expected as the pre-chamber ignition starts from the outer areas of the main chamber compared to the SI case with combustion starting from the center of the cylinder where the flame is more likely quenched on the cylinder walls. Moreover, the HC emission is the main drawback of the lean operation with the active pre-chamber. Generally, no significant difference is observed between different pre-chamber configurations. Bureshaid et al. [85] also indicated that the effects of the TJI on the lean burn limit and exhaust emissions varied with engine speeds.

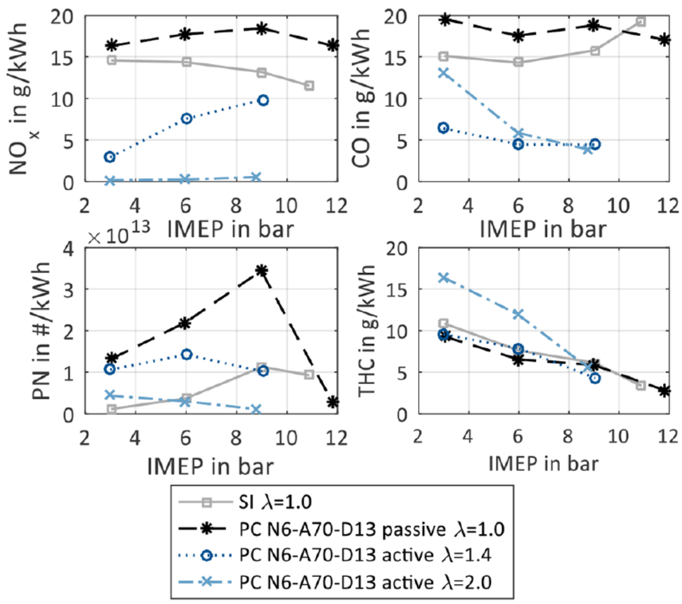

Figure 12. Effects of different ignition strategies on engine-out emissions at 1500 rpm [33].

Concerning the stoichiometric operation of the passive pre-chamber ignition system, a three-way catalyst is still mandatory to meet emission regulations. For the active pre-chamber ignition system operating at extreme lean conditions like the air-fuel ratio larger than 2, the raw NO_x and CO emissions are extremely low, an oxidation catalyst might be required to reduce the HC emissions [86]. If the air-fuel ratio is not large enough to reduce the raw NO_x and CO emissions, a lean-NO_x after-treatment and oxidation catalyst are required. However, this kind of design increases the cost of the after-treatment system significantly and is not economically feasible for commercialization. To the best of the authors' knowledge, there is no study on the SCR catalyst adopted on the gasoline engine equipped with a pre-chamber ignition system.

3 Design of the pre-chamber ignition system

The design of the pre-chamber ignition system needs to be seriously evaluated as it determines the scavenging and combustion inside the pre-chamber, the behavior of the jet ejection, and the combustion characteristics in the main chamber. Considering the whole engine operating map from cold start-up to full load, a compromise design should be made, and some benefits at part loads are sacrificed for high load knock mitigation [87]. Thus, the pre-chamber design could be very complex, and geometry sensitivities at the normal operating conditions are necessary to be conducted.

3.1 Pre-chamber design

The pre-chamber design involves lots of geometric parameters, like the pre-chamber volume, shape, orifice number, orifice diameter, spark plug location, and additional fuel injector for the active configuration [88]. To ensure a quick retrofit solution for the conventional spark plug, minimizing modifications to the cylinder head is one of the important design criteria for the pre-chamber. This makes the plug-and-play design to be a preferred solution. Thus, similar geometries for both the passive and active pre-chambers were normally present in laboratory researches. Considering the auxiliary fuel injection system; the complexity, size, and cost of the active pre-chamber are relatively high compared to those of the passive pre-chamber. Detailed design criteria of different components in the pre-chamber will be discussed in the following sections.

3.1.1 Pre-chamber volume

The pre-chamber volume determines the magnitude of mixture energy accessible for combustion. A large volume of the pre-chamber means more fuel is consumed to provide energy for the ignition and charge motion in the main chamber. The turbulent jets impinging on the main chamber wall might also occur with higher ignition energy. On the contrary, less fuel is required in a small pre-chamber to ensure steady combustion and maintain higher system efficiency. Since the jet ejection process generally occurs during the end of the compression stroke, the increased amount of charge in the main chamber might increase the compression power. Thus, the burned fuel inside the pre-chamber does not contribute to the engine output power. Therefore, minimizing the amount of fuel trapped inside the pre-chamber is preferred from the thermodynamic perspective.

Generally, the volume of the pre-chamber lies in the range from 2% to 6.5% relative to the clearance volume of the main chamber volume at the TDC. As the diameter is constrained by the cylinder head, the pre-chamber volume is normally adjusted by its length. To avoid modification to the engine, design constraints like a narrow throat diameter could deteriorate flow characteristics in the pre-chamber. As illustrated in Fig. 13, a Y shape design of the active pre-chamber that incorporates the spark plug on one side of the branch and the fuel injector on another side is commonly adopted. Both components are flush-mounted at the top of the pre-chamber [44, 80, 89].

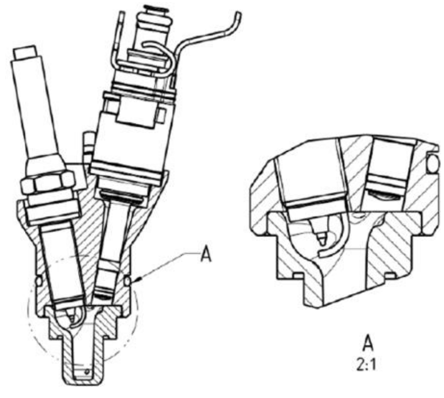

Figure 13. Cross-sectional view of a typical active pre-chamber [44].

The pre-chamber volume also has a direct effect on the effective CR of the engine. For the plug-and-play design, the effective CR decreases linearly with the increase of the pre-chamber volume. In addition, the pre-chamber volume could also play an important role in determining the turbulence level inside the pre-chamber. Serrano et al. [12] conducted CFD studies on pre-chamber designs with a larger volume of 1611 mm^3

and a smaller 1080 mm^3. Comparison results indicated that in a large pre-chamber, a tumble motion is developed, and a high TKE-level is expected in the upper segment of the pre-chamber. The reduced pre-chamber volume might also lead to a reduced TKE level at the spark plug.

3.1.2 Nozzle design

The nozzle connecting the pre-chamber and the main chamber serves to quench the flame, accelerate the burning products, and distribute the ignition sites in the main chamber. Thus, it plays a significant role in determining the pre-chamber emptying time, the nozzle flow velocity, the jet induced turbulence, and the jet structure. With respect to the nozzle design, the orifice diameter, number, and angle are key parameters that should be seriously selected. Since decreasing the pre-chamber volume and increasing the orifice diameter normally have the same effects on residual gas fraction, TKE, and scavenging quality, a derived parameter defined as the ratio of the total cross-sectional area of the holes to the pre-chamber volume (A/V ratio) is also widely used to characterize the pre-chamber geometry. Other parameters, like the nozzle length, have limited impacts on the pre-chamber flow and combustion.

The orifice diameter first determines the scavenging process in the pre-chamber. A small orifice diameter means an increased pressure loss across the nozzle. This reduces the gas exchange between chambers, and a poor mixture preparation featured with a large amount of residual gases trapped inside the pre-chamber is expected. On the contrary, a large hole diameter means a rapid loss of air-fuel mixture after the combustion starts in the pre-chamber [90]. The orifice diameter secondly determines the flame quenching. This has been discussed in Section 2.2. With a large pre-chamber orifice, the jets behave more like a torch combustion system. Optical engine tests conducted by Bunce et al. [60] showed that CH* is more prevalent in the jets of those designs with large orifices. The larger orifice does not quench the flame of pre-chamber combustion as effectively as the smaller orifice. However, a too small orifice could fail to create any ignition site in the main chamber. The orifice diameter thirdly determines the jet velocity. Driven by great chamber pressure disparity, a smaller orifice area leads to an increased jet velocity, which correlates to long jet penetration prior to ignition and shorter burn duration. The jet penetration should be controlled to minimize the distance each flame front traveling to consume the charge. Thermal efficiency could be maximized by targeting jet velocity.

It should be noted that the optimal orifice diameter is closely related to the engine operating condition. Test results obtained by Bunce et al. [42] indicated that at high loads, there exists an optimum orifice area range where knock is mitigated and combustion phasing can be advanced. The plateauing of the knock reduction potential of the small area geometries is likely due to the choked flow and reduced jet reactivity, which could be supported by the poor lean limit extension and combustion efficiency. On the contrary, a large orifice area means a very slow jet velocity, and combustion phasing is adversely affected. With respect to the low load conditions, nozzles with small areas are preferred to drive the jet velocity and penetration, and enhanced ignition site distribution and shorter burn duration are expected. Thus, the hole diameter should be selected considering the compromising of the pre-chamber scavenging and combustion for the engine map.

The orientation of the orifice inside the cap also plays an important role. First, the orifice angle should be selected to avoid pre-chamber jet impingement. Second, offsets in the lateral and vertical directions are preferred to generate swirling flow motion in the pre-chamber [33]. Meanwhile, the dissipation loss during the gas scavenging process can be decreased significantly, and the turbulence level can reach more than double the level of the conventional pre-chamber design. Thus, the pre-chamber designed with swirled orifices provides an increased turbulence level and a more robust combustion behavior [12]. CFD simulations of an active pre-chamber adopted on a rapid compression expansion machine (RCEM) conducted by Bolla et al. [91] indicated that the orientation of the orifice has a profound impact on the spatial distribution of fuel concentration and turbulence intensity around the spark plug. The tilted orifices could generate an outer swirling flow which leads to a fuel-rich counter-vortex in the central axis of the pre-chamber. On the contrary, the straight orifices lead to a leaner but more turbulent mixture around the spark plug. Tang et al. [59] suggested that the location of the pre-chamber orifice should also be evaluated seriously in the pre-chamber design. With an active pre-chamber designed with two rows of nozzle orifices arranged along the radial direction evenly, visualization results obtained on an optical engine fueled with methane showed that only jets from the lower-row orifice are intense enough to penetrate to the region close to the cylinder wall and to produce a distinct reaction zone.

With the total jet hole cross-section kept constant, Müller et al. [18] compared different jet hole designs shown in Fig. 14 (a), which include a conventional 4-hole design, a CFD-optimized 4-hole design, and a CFD-optimized 6-hole design. Compared to the conventional 4-hole design, the CFD-optimized 4-hole design and 6-hole design are featured with small side offsets but significant height offsets to introduce swirl in the pre-chamber. Fig. 14 (b) presents the normalized TKE at the spark plug with different jet hole designs. It is observed that the TKE level in the conventional pre-chamber is the smallest, and the peak TKE generated by the CFD-optimized 6-hole pre-chamber is roughly 50% higher than that of the CFD-optimized 4-hole pre-chamber. Thus, the optimized 6-hole design shows the maximum potential for lean-burn operation. However, the increased turbulent charge motion would also complicate the inflammation in the pre-chamber. This means a higher demand for the ignition system is mandatory.

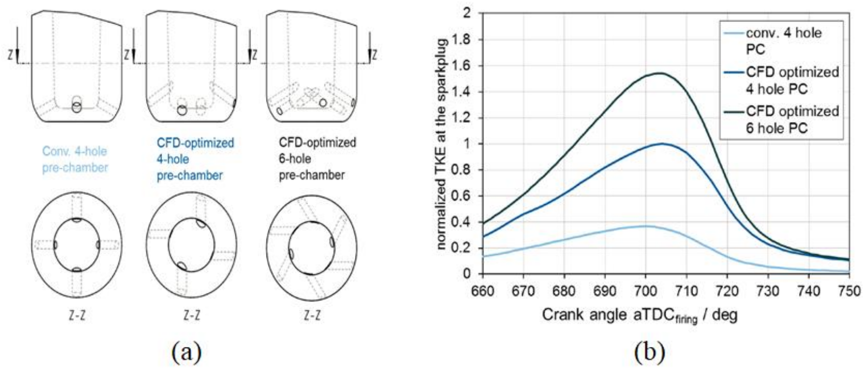

Figure 14. (a) Different pre-chamber designs and (b) the normalized turbulent kinetic energy at the spark plug [18].

3.1.3 Spark plug

The spark plug design involves variations in spark plug type, orientation, location, and electrode gap. Manipulating the spark plug design is assumed to have a big influence on flame kernel development and thus combustion processes in a conventional spark ignition combustion system [92]. However, the TJI combustion depends less on the spark plug design, as long as the combustion inside the pre-chamber can be initiated [93]. This is partly because the spark discharge occupies a much larger fraction of the chamber relative to the convention spark ignition. Meanwhile, combustion in the main chamber is mainly driven by the chemical, thermal, and turbulence effects of the jets, as discussed in Section 2.3.1.

Attard et al. [94] evaluated the effects of the ignition energy ranging from 75 to less than 5 mJ on the combustion performance of an active pre-chamber. Gasoline and propane were used as fuels for the main chamber and the pre-chamber, respectively. Test results of the minimum ignition energy required to support jet ignition combustion at varying dilution levels indicated that the minimum ignition energy is smaller than 10 mJ when the exhaust lambda falls in the range of 0.9 to 1.9. On the contrary, much higher ignition energy is demanded to support the pre-chamber combustion at the lean and rich operating limits. Experimental results also highlighted that the pre-chamber ignition is largely unaffected by the variation of the ignition energy compared to the conventional SI engine. Therefore, it is possible to reduce the ignition energy demand and hence ignition coil and spark plug size for the pre-chamber ignition system. This in turn benefits the component longevity, cost, and cylinder head packaging.

3.1.4 Auxiliary fuel injection

The active pre-chamber ignition system characterized by an additional low-flow fuel injection system provides another degree of freedom for controlling the mixture in both chambers. Gaseous fuels like methane, hydrogen, and propane are usually adopted to get better mixture formation in an active pre-chamber because of the reduced momentum of the liquid [24, 95]. This means an additional fuel tank and a specific dosing/injection system are mandatory for the pilot fuel. Therefore, liquid gasoline injection remains to be the best candidate to develop a practical TJI concept for passenger car applications [18].

In general, direct injection of gasoline brings challenges like spray target, mixture formation, and dosing of a very small amount of liquid fuel [12]. Considering the low fuel flow rate and short injection duration, a shot-to-shot deviation is expected for the pre-chamber injector. Meanwhile, the existing direct injection system is not designed for such a small amount of fuel, and the measure of the mass flow rate injected into the pre-chamber might be inaccurate with conventional direct injection fuel injectors. To develop a prototype low-flow injector, modifications comprising reducing the injection pressure and altering the injector nozzle tip are normally adopted on a production-based solenoid direct injector [82].

The injection timing needs to be carefully evaluated considering the air-fuel mixture formation in the pre-chamber. Hua et al. [78] indicated that the injection timing in the pre-chamber should be set in the early stage of the compression stroke to provide a proper fuel-air mixture in the pre-chamber and to avoid the diffusion of fuel from the pre-chamber to the main chamber. As illustrated in Fig. 15, CFD results obtained by Bunce et al. [42] testified that an early fuel injection leads to “over-mixing” inside the pre-chamber due to the increased vaporization and mixing time. This can produce an overly dilute mixture near the spark plug and thus pose a risk of misfire. Concerning the low background pressure in the pre-chamber at the early injection timing, a significant quantity of auxiliary fuel might exit the pre-chamber before the spark timing. Late fuel injection in the compression stroke is preferred to guarantee an ignitable mixture near the spark plug and maximize the quantity of auxiliary injected fuel involved in the pre-chamber combustion event. However, a late fuel injection might not provide sufficient time for good vaporization. Thus, the fuel injection timing should be optimized seriously according to the injector location, amount of injected fuel, lambda level, engine load, etc.

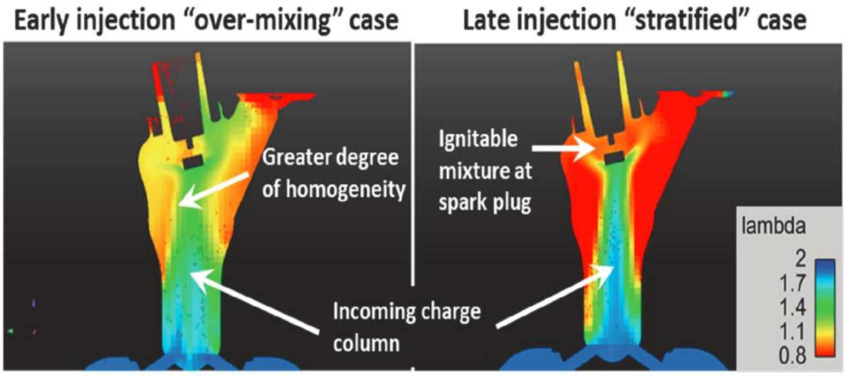

Figure 15. Mixture preparation with early (left) and late fuel injection (right) timing in the pre-chamber at the time of the spark with constant pre-chamber fuel quantity [42].

The amount of fuel injected into the pre-chamber is another key operating parameter since it determines the pressure rise and the combustion duration in the pre-chamber. In general, this parameter is mainly determined by the pre-chamber volume and the pre-set air/fuel ratio to maintain the combustion stability (like COV of IMEP <3%). Attard et al. [96] demonstrated that the optimum amount of fuel injected into the pre-chamber for maximum burn rate enhancement allows a slightly rich pre-chamber combustion event, which has been proved to benefit the production of radicals. However, extremely rich pre-chamber cases with pre-chamber lambda smaller than 0.4 normally result in a longer ignition delay and relatively slower pressure rise inside the pre-chamber [97].

To maintain combustion stability, the amount of auxiliary fuel should also be increased with the increasing lambda level in the main chamber. Experimental studies on the impacts of lambda and pre-chamber fuel quantity on pre-chamber and main chamber combustion were conducted at the BMEP of 6 bar @ 1500 rpm by Peters et al. [50]. The results indicated that the auxiliary fuel added in the pre-chamber should be increased with the increase of the main chamber lambda, and a similar overall pre-chamber lambda should be kept to maintain combustion stability in the main chamber.

Attard et al. [45, 98] investigated pilot fuel injection parameters on a retrofitted single-cylinder thermal engine. Experiments were conducted at 1500 rpm with the lambda of 1.8 and the spark timing fixed at 25 CAD before TDC. The pre-chamber and main chamber were fueled with gaseous propane and gasoline, respectively, and the total fuel energy was also kept constant at different points. It is concluded that there exists an optimum pre-chamber fuel flow to achieve the best net IMEP and combustion stability. Besides, this optimal value is heavily dependent on the dilution level since more pre-chamber fuel is required to maintain combustion stability with the increasing dilution level. Concerning the end of injection timing inside the pre-chamber, the optimal value falls in the range of 70~80 CAD before TDC, which is around 50 CAD prior to the spark discharge. This is mainly because this period provides sufficient time for charge mixing and still restrains the pilot fuel inside the pre-chamber. It is also noted that compared to the engine net IMEP, combustion stability is more sensitive to the fuel injection parameters.

The injection orientation which determines the fuel evaporation and mixture preparation is another key design parameter. Serrano et al. [12] compared two different concepts of fuel injection. As shown in Fig. 16, the injection orientation in the first concept is selected to achieve the maximum length of the injection path. This design aims at realizing a moderate residual gas scavenging and a high mixture homogenization with minimum wall film formation. The injection jet in the second concept is close to the spark plug in order to directly affect the air-fuel mixture at the spark plug. The fuel injection timing and quality are fixed at 259 CAD before TDC and 1.44 mg in concept 1 and 59 CAD before TDC and 0.6 mg in concept 2. CFD results indicated that the second concept with a smaller fuel injection quality and a higher injection pressure achieves a good air-fuel mixture near the spark plug before the TDC, which is quite similar to that in the first concept.

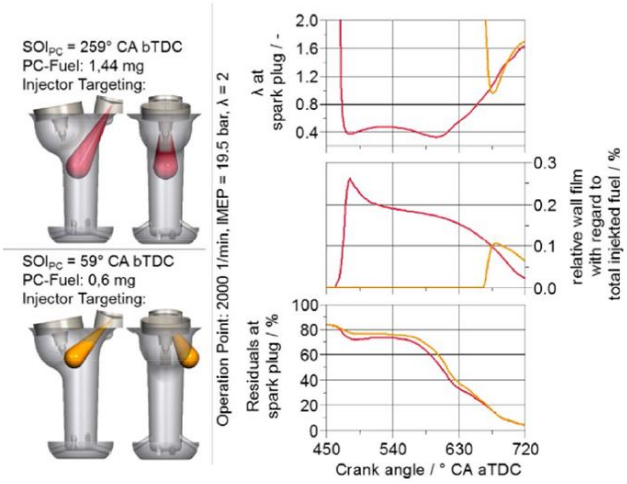

Figure 16. Comparison of different fuel injection strategies [12].

3.2 Fuel and air management for the main chamber

As the combustion mode is changed with the adoption of the pre-chamber ignition system, fuel and air management for the main chamber should be updated to maximize the potential of the pre-chamber ignition system.

3.2.1 Fuel injection for the main chamber

The main chamber can be fueled with PFI or GDI fueling hardware. Considering the packaging constraints of the central pre-chamber, the direct injection is normally implemented laterally. Thus, it is not a good choice. In addition, the GDI injection system always leads to a poor lambda distribution in the main chamber compared to the PFI. Although the cooling effect of gasoline evaporation with GDI results in better combustion timing, this effect is less attractive since knock resistance is strongly improved with TJI.

Experimental research aiming at comparing the GDI and PFI fueling for the main chamber operating under lean-burn conditions was conducted by Serrano et al. [12]. The results showed that the PFI is found to be better than the GDI considering the trade-off between efficiency and pollutants at the IMEP of 13 bar @ 3000 rpm. The optimal combustion phasing can be obtained with the GDI cooling effect, while the PFI can only achieve the optimal combustion phasing at a lambda value larger than 1.7. At a high lambda level, the PFI strategy shows a better fuel economy performance due to the higher combustion efficiency, as testified with the variations of unburned HC and CO. Compared to the GDI counterpart, the homogeneous mixture with PFI could benefit the combustion duration at the lambda value larger than 1.7. Thus, the authors concluded that the PFI is preferred for the main chamber injection.

The variation of the fuel consumption depends on many factors like the pre-chamber design, air management, and load control. In general, low fuel consumption is expected in the main chamber with the TJI, especially when the active TJI system is adopted. It should be noted that this decrement in fuel consumption is not large enough to change the design criteria for the fuel supply system. Meanwhile, optimizing the parameters of fuel injection for the main chamber has limited effects on the engine performance since the ignition energy is largely improved by the turbulent jets.

3.2.2 Port design

In the conventional SI engine, the flame propagation strongly relies on the in-cylinder tumble motion and TKE. Employing high tumble intake ports and valve profiles can benefit the flame propagation and reduce the combustion duration, but leads to higher flow losses and pumping work [12]. With respect to the TJI, flame propagation in the main chamber is primarily related to the jets coming out through the pre-chamber orifices. In addition, the enhanced flow in the main chamber does not promote the initial flame kernel growth in the pre-chamber. Thus, the demand for the charge motion is not very high from the perspectives of the main chamber and pre-chamber combustion.

The tumble motion also influences the mixture preparation process. Spatial variations of the AFR are acceptable when the engine is operated with stoichiometric mixtures for both the PFI and DI gasoline engines [99]. In the case of lean-burn combustion with the AFR of up to 2, mixture preparation should be as homogenous as possible to avoid an extremely lean area where the flame propagation might be terminated. Thus, a moderate tumble motion is still mandatory for the lean burn combustion, especially with the GDI system. Further considering ultra-lean conditions, the flow capacities of the intake system should also be improved to reduce the scavenging loss and guarantee the power density. Therefore, the intake port is normally redesigned with a higher flow capacity and a moderate tumble motion.

Bunce et al. [42] evaluated different charge motion cases including the baseline, increased tumble, introduction of swirl, and a combination of swirl and tumble. The results showed that an increased tumble could improve the indicated and brake thermal efficiency by 0.5-1 percentage point, which is a measurable increase in efficiency purely through the adjustment of intake port-induced charge motion. Thus, integrating a higher tumble intake port is promising in improving the TJI.

3.2.3 Turbocharging system

The operating strategies of the TJI system also have big influences on the boosting requirement. To fully utilize the benefits of knock mitigation with passive TJI, other engine tuning strategies, like the increased CR, EGR, and Miller cycle, are always adopted. For the active TJI operating under lean conditions, the boosting system needs to support enough scavenging air to the main chamber. Meanwhile, the low exhaust enthalpy at lean-burn conditions put forward high demands for the boosting system, like minimizing the exhaust backpressure and being compatible with the low exhaust temperature. Finally, the boosting system needs to be upgraded to enable the map-wide lean/ultra-lean operation and multiple operating strategies. However, current studies seldomly address the rematching of the turbocharging system for the pre-chamber ignition system.

4 Summary of the pre-chamber ignition in the gasoline engine

Due to the unquestionable advantages of the TJI, recent years have witnessed a growing number of computational studies and experimental campaigns aiming at providing insights into relationships between jet ignition and engine performance. A summary of selected research works is presented in Table 2. It can be safely concluded that the TJI system combined with other complementary technologies, like the increased CR, Miller cycle, and cooled EGR, has great potential in improving the fuel consumption, and the improvement varies with the selected operating condition. Moreover, the passive and active configurations have their own special applications. A more detailed review will be conducted in the following sections.

Table 2. Overview of selected research works on the pre-chamber ignition system.

Affiliation/ Refs.	Research methods	Engine specifications/ model descriptions	Pre-chamber specifications	Parameter tuning and engine optimization	Key findings
IAV [75]	CFD and single-cylinder engine test	A 0.5 L single-cylinder engine with the CR of 10, 12, 13; transient k-ε models adopted in Star-CD	Optimized active and passive pre-chamber configurations obtained by CFD studies	The TJI integrated with the increased CR, EGR, and Miller cycle strategies were evaluated at both part loads and high loads.	By adopting the active version at low loads and the passive version at high loads, the pre-chamber ignition combined with the increased CR (+2) and external cooled EGR provides a fuel economy benefit of 2~6%.
Mahle [50, 74]	Optical test and multi-cylinder engine test	Schlieren and OH* chemiluminescence obtained on an optically accessible single-cylinder engine; 1.5L 3-cylinder engine with the CR of 9.25:1	Geometry sensitivities were evaluated to identify the active and passive pre-chamber configurations at different loads	Sweeps of lambda and pre-chamber fuel quantity were conducted on the active version. Effects of the Miller cycle, external cooled EGR, and increased CR on the TJI were evaluated.	With optimized lambda and pre-chamber fueling, the active version could result in a peak brake thermal efficiency larger than 42%. The passive configuration combined with the increased CR, Miller cycle, and EGR strategies generates a minimum BSFC of 207 g/kWh at 12 bar BMEP @ 3000 rpm.
CMT [41, 90]	0D, 1D, 3D CFD, and single-cylinder engine test	A PFI 0.404L single-cylinder engine with the CR of 13.4:1; RANS based turbulence model and ECFM model adopted in Converge code.	Different pre-chamber designs were evaluated with CFD simulations. Two extreme designs were evaluated with the single-cylinder test.	Pre-chamber designs were experimentally validated at high load/speed conditions (4500 rpm, 12.5 bar IMEP). EGR and air dilution strategies were evaluated.	The heat losses across the pre-chamber walls are negligible (<5%) compared to the overall energy balance inside the pre-chamber. The maximum air dilution level with the passive TJI system is similar to that of the convention SI engine.
IFPEN [12]	Single-cylinder engine test and 3D	A 0.408L single-cylinder engine with CR of 15:1 was adopted; mixture formation evaluation	Pre-chamber volume, jet holes, and spark plug location were optimized. Gas and	Sweeps of lambda were tested at 13 bar IMEP @ 3000 rpm. Both PFI and side-mounted DI were considered. Fuel injection timing	A maximal indicated thermal efficiency of 47% was achieved at the lambda of 2. The optimal fuel mass flow rate injected into the pre-chamber was the minimal fuel quantity

	CFD study	conducted in Star-CD code.	gasoline as pilot fuels were evaluated.	and mass flow rate of the pre-chamber were checked.	that the pre-chamber injector can deliver.
Bosch [40]	3D CFD and multi-cylinder engine test	2.0 L, inline four-cylinder, turbocharged DI central mounted engine; RANS based 3D CFD in AVL Fire	18 designs with variants of volume, orifice number, diameter, and orientation	The influences of geometrical parameters on scavenging, turbulence generation, and air-fuel mixture were evaluated at IMEP 3bar @ 1500 rpm and IMEP 8 bar @ 2000 rpm.	Decreasing the volume or increasing the hole diameter helps increase the scavenging quality but deteriorates the turbulence level. The CFD ranking of pre-chamber designs without combustion displays significant discrepancies with the engine test ranking.
FEV [18]	Single-cylinder engine test	0.399 L single-cylinder engine with geometrical CR of 11~16	The active pre-chamber was optimized with CFD studies, and pilot fuels of gasoline, CNG, and H_2 were evaluated.	A lateral DI injector position was chosen to ensure an optimum central position of the ignition system. Three load points were selected, which are most relevant for hybrid operation.	With the optimized pre-chamber configuration, a large air/fuel-ratio window of stable combustion can be achieved. Hydrogen as the pilot fuel has the advantage of particulate emissions but with low overall efficiency.
KAUST [51, 87, 97, 100, 101]	1D, 3D, and optical test	A single-cylinder optical engine was modified based on a heavy-duty 6-cylinder engine with the main chamber supplied with ethanol or methane.	A narrow-throat pre-chamber fueled with methane is designed with a volume of 1.6~3.4% of clearance volume and two rows of six nozzle holes.	The engine was operated at 1200 rpm with an intake pressure of 1 bar. Tests of global lambda sweeps with constant fuel flow or air flow were conducted.	The throttling effect arisen from the narrow throat leads to excessive quenching and thus reduces the reactivity of combustion products. A flow reversal pattern is observed and leads to a second heat release. The passive version exhibits a random and sequential jet emergence.
ETH [55, 56]	3D CFD and optical test	Methane fueled RCEM; Revised G-equation combustion model based on RANS	Passive pre-chambers with different inner volumes but the same nozzle diameter of 1.2 mm	Conditions in the RCEM are tuned to be close to the engine operation at 1000 rpm. Variations of lambda, turbulence level, and initial temperature were checked.	The jet head tends to be more reactive than the jet stem because of the higher turbulence level and larger eddy size. The flame jets have very small Damköhler numbers but increase over time.

Technische Universitat Munchen [33]	Single-cylinder engine test	0.463L single-cylinder engine with a side-mounted direct injector	Gasoline-fueled pre-chambers with four different orifice configurations	Variations of pre-chamber geometries, Lambda, engine load, and geometrical CR were evaluated at 1500 rpm.	The active pre-chamber extends the lean limit from lambda of 1.4 to 2.0. A peak efficiency of 43% is achievable with NO_x emissions dropping down to 0.2 g/kWh.
Politecnico di Bari [52]	Optical test and 3D CFD	Optically accessible 0.25L single-cylinder PFI engine with port-injected methane and air	Four-hole pre-chambers with volumes of 6% of the clearance volume	Tests at 2000 rpm were conducted to calibrate the fired and unfired CFD simulations using Converge code.	The TJI can achieve a double maximum pressure and a 6-times faster combustion speed compared to those of the standard one.
Tianjin University [77]	Single-cylinder engine test	0.5L direct-injected single-cylinder gasoline engine	Three types of pr-chambers with different volumes and numbers of holes	The engine was operated at 1500 rpm with the lambda ranging from 1.0~2.3, and pre-chamber injection timing was evaluated.	The optimum injection timing for the pre-chamber is around 180 ˚CA bTDC. The single-hole pre-chamber generates stronger hot jets than the 7-hole pre-chambers
Michigan State University [83]	single-cylinder engine test	0.55L port fueled single-cylinder prototype engine with the compression ratio of 13.3:1	A pre-chamber with auxiliary air/fuel supply and volume of 6 % of clearance volume	Engine tests were performed at 6 bar IMEPg @1500 rpm, which is the highest load achieved at naturally aspirated conditions maintaining a 40% EGR rate.	The excess air dilution provided slightly better thermal efficiency compared to EGR dilution, and the maximum EGR tolerance of 40% is probably limited by the poor pre-chamber ignitability.
Istituto Motori CNR [84]	Optical test	An optical port fueled gasoline engine equipped with methane fueled pre-chamber	A four-hole pre-chamber with the volume of 7.2% of the clearance volume	The engine runs at 1500 and 2000 rpm at wide-open throttle in stoichiometric and lean operation conditions (lambda of up to 1.6).	At lean operation conditions, each turbulent jet shows a specific behavior in terms of flame speed due to the inhomogeneity in the main chamber.
University of Naples “Federico II” [102]	Single-cylinder engine test and 1D simulation	CNG or H_2 fueled active pre-chamber, gasoline DI main chamber, and refined phenomenological sub-models.	Four-hole pre-chambers with volumes of 3.6% of the clearance volume and A/V of 0.033 cm^{-1}	39 operating points were tested at lambda and load sweeps, and the spark advance is tuned to realize the optimal combustion phasing.	H_2 as the auxiliary fuel only leads to engine benefit at very lean conditions. The lean-burn limit with the passive pre-chamber is less extended.

Università degli Studi di Firenze [103]	Engine test	A low-pressure direct-injected 2-stroke 50 cm^3 engine for motorcycle use	Two passive pre-chambers with the volume of 5.07% of the clearance volume	Experiments were performed from 3000 to 8500 rpm at engine full load.	The pre-chamber can solve combustion stability issues of small 2-stroke engines. A decrease of up to 85% in the cycle-to-cycle variation is observed with bigger orifices.
Aramco Research Center [104]	Multi-cylinder engine test	2.2 L Miller cycle GDI engine is designed with a compression ratio of 14:1, and methane is used as the auxiliary fuel.	Passive and gaseous active pre-chambers with different nozzle diameters, number of holes, and volumes	Tests were conducted at a high usage part load of 5 bar BMEP @1500 rpm, and a range of excess air and EGR diluted conditions were evaluated.	The incomplete scavenging and increased heat transfer loss of the passive pre-chamber restrict the EGR tolerance. The optimal engine efficiency occurs at the lambda 0f 1.7 to 1.8 with the active pre-chamber.

4.1 Simulation research

Computational tools based on 0D, 1D, and 3D numerical methods are preferred to overcome the limitations of test studies for the design of the pre-chamber. The 3D CFD is selected to accurately describe the interaction between combustion, chemical kinetics, and turbulence in a TJI engine. However, the 3D simulation is normally limited to a reduced number of operating points due to the computational effort. By adopting proper phenomenological sub-models for in-cylinder turbulence and combustion, the 0D/1D simulation is capable of investigating a large number of operating conditions with reduced computational effort. Aims of 0D and 1D simulation include preliminary pre-chamber design, identification of operating conditions, providing boundary conditions for 3D CFD simulation, understanding observed trends from engine experiments, and engine control purposes [105, 106].

4.1.1 Simplified 0D and 1D simulation

Simple 0D simulations are suitable for evaluating qualitative trends of the flow between the main chamber and pre-chamber and performing parametric studies of different geometrical details like volume and orifice diameter [54]. The pre-chamber and the main chamber in the 0D simulation are normally simplified as two separate control volumes connecting through a small orifice. Using energy conservation and ideal gas law equations, thermodynamic processes in those two chambers can be depicted as,

$$m_{MC}c_{v,MC}\frac{\partial T_{MC}}{\partial t}=\frac{\partial Q_{MC}}{\partial t}-p_{MC}\frac{\partial V_{MC}}{\partial t}-\frac{\partial m_{MC}}{\partial t}(h_{out}-e_{in}) \tag{1}$$

$$p_{MC}\frac{\partial V_{MC}}{\partial t}+V_{MC}\frac{\partial p_{MC}}{\partial t}=m_{MC}R\frac{\partial T_{MC}}{\partial t}-T_{MC}R\frac{\partial m_{MC}}{\partial t} \tag{2}$$

$$m_{PC}c_{v,PC}\frac{\partial T_{PC}}{\partial t}=\frac{\partial Q_{PC}}{\partial t}+\frac{\partial m_{PC}}{\partial t}(h_{out}-e_{in}) \tag{3}$$

$$p_{PC}\frac{\partial V_{PC}}{\partial t}+V_{PC}\frac{\partial p_{MC}}{\partial t}=m_{PC}R\frac{\partial T_{PC}}{\partial t}-T_{PC}R\frac{\partial m_{PC}}{\partial t} \tag{4}$$

where subscript 'MC' and 'PC' indicate the averaged state parameters inside the main chamber and the pre-chamber, respectively. 'h' and 'e' are the enthalpy and internal energy, respectively.

To obtain an accurate instantaneous heat release rate as well as proper control of the equivalence ratio in the pre-chamber at the spark timing, an accurate calculation of the gas exchange between those two chambers is mandatory. Here, the compressible flow through an isenthalpic orifice is normally adopted [54, 107, 108],

$$\dot{m}_e(t) = C_D A_{nz} \frac{p_{in}(t)}{\sqrt{R_{in} T_{in}(t)}} \left(\frac{p_{out}(t)}{p_{in}(t)}\right)^{1/\gamma} \left\{\frac{2\gamma}{\gamma - 1}\left[1 - \left(\frac{p_{out}(t)}{p_{in}(t)}\right)^{(\gamma-1)/\gamma}\right]\right\}^{1/2} \tag{5}$$

where C_D is the discharge coefficient of the orifice, and A_{nz} indicates the equivalent flow area of the nozzle. Since the discharge coefficient drastically influences the mass flow rate, velocity, and turbulence generation, linking this coefficient with certain pre-chamber geometries and operational parameters is important. Meanwhile, this parameter depends on the pressure ratio across two chambers and relates to the mixture density [54]. Thus, it remains to be a big challenge to determine the discharge coefficient. It is also noted that the pressure difference between the pre-chamber and the main chamber at the peak level might lead to a choked flow [42]. With the assumption of ideal gas behavior, the choking flow condition at the orifice is defined by,

$$\frac{p_{out}}{p_{in}} = \left(\frac{2}{\gamma + 1}\right)^{\gamma/(\gamma+1)} \tag{6}$$

where γ is the polytropic coefficient of the mixture in this case. Bunce et al. [60] evaluated five different pre-chamber designs with the normalized nozzle orifice area ranging from 0.27 to 2.48 on an optical engine. Visualization results showed that the luminous jets emerging from small orifices fail to create any ignition site in the main chamber. The author attributed this phenomenon to the choked flow resulting from the big pressure discrepancy between those two chambers. Therefore, the restricted mass flow rate with a lower energy density curtails the effectiveness of the TJI. By adopting Eq. (6), the choked durations are estimated to be 3~4 deg crank angles.

Heat losses should be seriously checked due to the large surface to volume ratio of the pre-chamber. It is noted that the flow field inside the pre-chamber is driven by the nozzle velocity instead of the piston moving. This indicates that the characteristic velocity in the heat transfer correlation should be addressed to account for the turbulence intensity. As there is no specific heat transfer model for the pre-chamber heat transfer, a modified Woschni's correlation shown below is normally suggested for the pre-chamber [109],

$$h_{w,PC}\left[\frac{W}{m^2K}\right] = c_{ws}D_{PC}[m]^{-0.2}p_{PC}[bar]^{0.8}T_{PC}[K]^{-0.53}w_{w,PC}[m/s]^{0.8} \quad (7)$$

where the characteristic velocity $w_{w,PC}$ during the compression stroke is expressed as a function of the mean piston speed $\bar{u}_p$ and expressed by [109],

$$w_{w,PC} = 2.28\bar{u}_p \quad (8)$$

Combustion inside the pre-chamber and main chamber can be modeled with different methods. One easy solution is using the calculated heat release rate from the experimental pressure trace. Test data in published works showed the pre-chamber ignition system normally decreases the combustion duration by 2 and 3 times of that in the conventional SI engine. A Wiebe function combined with a scaling factor could be adopted and adjusted to generate the desired combustion profile and duration in the main chamber [90, 107].

Another predictive but complicated combustion model is based on the active flame front area and a turbulent flame speed to predict the heat release rate in the TJI system. Thus, the single-zone assumption for the control volume is not sufficient, and the pre-chamber volume needs to be separated into two zones which include a burned zone behind the flame front and an unburned zone ahead of the flame front [110]. Turbulence intensity inside the pre-chamber could be modeled with a refined 0D turbulence sub-model or via a reduction of the well-established CFD $k-\varepsilon$ model [54]. A detailed description of the predictive combustion model will not be presented here due to the limited article length but can be referred to works conducted by Bardis et al. [54] and Hiraoka et al [109].

Bardis et al. [54] suggested that a well-developed 0D phenomenological model can accurately predict many key parameters including the pressure difference between the two chambers, the turbulent intensity, the integral length scale, the temperature traces, as well as the nozzle flow velocities for all the examined cases. Bozza et al. [111] developed a new quasi-dimensional model for the basic phenomenon in an active pre-chamber engine. Combustion in both the pre-chamber and the main chamber was depicted in a two-zone schematization with a quasi-dimensional fraction model developed by the authors. However, the authors underlined that the fractal model is based on the theoretical background of the SI engine combustion falling in the wrinkled-corrugated flamelets domain. For the main chamber operating under diluted conditions, the laminar flame speed is low and the local turbulence is high at the first combustion stage. Thus, the combustion moves toward the thickened wrinkled flamelets or broken reactions. Therefore, both turbulence and combustion sub-models were modified to handle the divided combustion chamber architecture.

The calibration of the above 0D models describing in-cylinder conditions is always conducted by embedding them into a 1D code or commercial software. Also, a 1D simulation is mandatory to develop a map-wide operating strategy. Benajes et al. [90] built a 1D Wave Action Model of the experimental engine equipped with a pre-chamber. The pre-chamber is connected to the engine cylinder volume by a set of ducts representing the pre-chamber orifices. Combustion in the main chamber was simulated by imposing the heat release rate profile obtained from the experimental cylinder pressure. Since the pressure trace inside the pre-chamber was not available, combustion in the pre-chamber was modeled by tuning the shape parameters in the Wiebe function to match the desired combustion shape, and the duration was linearly scaled with the pre-chamber volume. The number of orifices was fixed at 6, whereas the pre-chamber volume ranged from 400 to 1000 mm^3 and the diameter of the orifices from 0.4 to 0.9 mm, these were evaluated by comparing the maximum pressure difference between those two chambers during the ejection event, the amount of fuel available at the spark timing, and the total burned fuel inside the pre-chamber. The results indicated that the optimum pre-chamber design should be a balance between the pre-chamber volume and the orifice area.

Hlaing et al. [87] used an engine cylinder template to simulate the pre-chamber and a user-defined object to lock the pre-chamber at the bottom dead center position throughout the cycle. An orifice object is adopted to mimic pre-chamber nozzles. The small throat diameter leads to high flow impedance and long residence time for the burned products flowing out of the pre-chamber, and the discharge coefficient of the orifice was found to be 0.33 with the three-pressure analysis. They also indicated that the throttling effect could result in excessive quenching, which further reduced the reactivity of the pre-chamber products.

Based on a validated one-dimensional model, Novella et al. [47] evaluated the effects of the passive pre-chamber design on the performance of a turbo-charged high-compression ratio Miller-cycle engine fueled by compressed natural gas. A trade-off trend between the pre-chamber swirl level which stabilizes the combustion and the pre-chamber scavenging determining the external EGR tolerance was identified. Bozza et al. [102] employed quasi-dimensional phenomenological sub-models in a 1D model to evaluate the mixture preparation, turbulence evolution, and flame propagation processes of a test engine. Considering the turbulence and burn rate enhancements in the main chamber due to the burned gas jets emerging from the pre-chamber, the numerical approach was testified to accurately reproduce the experimental data without requiring any case-dependent tuning of the model constants. Bellis et al. [112] extended an in-house developed phenomenological model to handle the pre-chamber architecture in the 1D GT-Power framework, which takes into account the turbulence and combustion in the main chamber initiated by the burned gas jets from the pre-chamber. The validation results against the experiment conducted on a single-cylinder engine and 3D simulations proved that engine performance, pressure traces, combustion parameters and pollutant emissions are accurately captured without requiring any case-dependent tuning of the model constants.

The potential of the positive thermal efficiency translated into real-world fuel economy should also be seriously evaluated. Attard et al. [113] developed a drive cycle model and evaluated different combustion modes including stoichiometric spark ignition, homogenous charge compression ignition (HCCI), and lean-burn jet ignition over NEDC and FTP driving cycles. Simulation results on a production level I4 PFI 2.4L GM engine indicated that the jet ignition system can provide a 13% improvement in fuel consumption across driving cycles compared to the baseline stoichiometric combustion system. The TJI matches the HCCI combustion model in fuel benefits but requires much less complicated hardware and a much simpler control system. Besides, the maximum improvement in fuel economy of 25% could be achieved when the jet ignition combustion is coupled with engine downsizing.

4.1.2 Sophisticated CFD works

To make better understandings of the scavenging, ignition, and flame propagation, CFD simulations should be adopted. In addition, CFD is normally used as an explanatory tool to drive the design and optimization of operating parameters, like predicting variations of the combustion process with geometric changes in either the main chamber or the pre-chamber. However, sophisticated CFD modeling of the pre-chamber is currently limited due to chemical and physical complexities. Meanwhile, some state-of-the-art models developed for the conventional SI operation might not be predictive at challenging conditions of the TJI system.

With respect to the turbulence modeling, the RANS based model which reproduces the mean behavior of the relevant parameters is normally selected over the LES model because of the simplicity and reduced computational time. In the published works, only limited simulations using the LES were reported, and most of them were conducted for rapid compression machines rather than metal engines [91, 114]. To compare those two different turbulence models in predicting the turbulence and fuel-air mixing, Bolla et al. [91] conducted numerical studies of an automotive-sized scavenged pre-chamber adopted on a RCEM. The results indicated that the RANS based model is capable of reproducing the main ensemble-averaged LES flow patterns with different pre-chambers.

Using the CFD code of VECTIS, Shapiro et al. [115] applied a novel spark model developed by Ricardo in the analysis of a pre-chamber ignition system adopted on a RCEM. This spark model covers all stages of spark discharge from breakdown to the formation of the initial kernel. The sensitivity analysis of this spark ignition model indicated that the uncertainties of model parameters alone could not account for the faster flame propagation observed by comparison with the experiment, and the turbulent flame speed used in the combustion model remains to be the key factor in influencing the flame jet propagation.

Since the flame propagation through the orifices is quite complicated, building a high-fidelity combustion model to capture flame dynamics across the pre-chamber nozzles is a big challenge [116]. Previous numerical research proved that the combustion is near the thick flames regime, especially at a high dilution rate. Thus, flamelet hypotheses are not fulfilled, and models like ECFM and G-Equation are not able to capture the combustion behavior of flame quenching through the orifice. This might lead to a shorter ignition delay in the main chamber. To the best of the authors' knowledge, only limited research works were reported with well-tuned combustion models [61, 62]. Although the physical phenomena of the TJI combustion are still not yet well established, model constants can be adjusted to correct the laminar flame speed and match the experimental pressure traces [41]. However, the capability of predicting all phenomena involved in the TJI combustion is uncertain.

To avoid possible numerical uncertainties and to assure a suitable analysis of the result, many researchers divided their studies into two stages, with the non-reacting or cold flow simulation focusing on the scavenging and filling processes and the reacting simulation of the closed cycle investigating the combustion and energy conversion processes. It should also be noted that if the simulation only aims at studying the mixing and the turbulent conditions inside the pre-chamber and main chamber, the incorporated combustion model with/without detailed chemical kinetics and proper treatment for turbulence-chemistry interaction in the flame propagation might not be a critical issue.

Benajes et al. [41] conducted a two-stage CFD study on a passive pre-chamber engine. Scavenging and turbulence distributions with different pre-chamber geometries were checked thoroughly. The extended coherent flamelet model (ECFM), which tracks the flame propagation by solving a transport equation, was adopted in the second-stage simulation. Detailed CFD simulations on combustion processes at ultra-lean conditions (lambda of 2) in a passive pre-chamber engine were conducted. The results indicated that the significant reduction in laminar flame speed inside the pre-chamber leads to low-quality jets. Further considering the external dilution strategies, the laminar flame speed and combustion rate will deteriorate in the main chamber. To recover the laminar flame speed and extend the air dilution limit, Benajes et al. [41] also evaluated some approaches of increasing the flow temperature, like pre-chamber insulation by using ceramic materials and pre-chamber heating with external energy sources. It was found that minimizing the heat losses across the pre-chamber walls only provides a marginal improvement in laminar flame speed, and external heating is not sufficient to guarantee suitable combustion in the main chamber. Thus, the passive pre-chamber ignition system only has a limited capacity for dilution combustion.

Silva et al. [51] built RANS based CFD model of a CH_4 fueled engine with the well-stirred reactor combustion model coupled with a methane oxidation mechanism. The effects of geometric parameters of the passive pre-chamber including the throat diameter, nozzle length, and nozzle diameter on combustion characteristics were evaluated. Validations of the CFD model were conducted by comparing pressure traces in both chambers under the motoring condition and at 1200 rpm. The results indicated that the throat diameter has a large influence on the pressure build-up and residence time inside the pre-chamber, while the nozzle diameter impacts both the peak pressure and residence time.

Distaso et al. [53] conducted 3D CFD studies on an active pre-chamber ignition system adopted on a lean-burn methane engine. Scavenging and combustion inside the pre-chamber were divided into six phases, including filling & scavenging, mixing, flame propagation, ejection, reburning, expulsion & extraction. Thelen et al. [39, 73, 117, 118] did lots of work dedicated to the CFD modeling of the TJI process. 3D CFD simulations with detailed combustion chemistry were conducted to study the effects of different orifice diameters of 1.0 mm, 1.5 mm, 2.0 mm, and 3.0 mm. Simulation results showed that the orifice with a diameter of 1.5 mm shows the fastest ignition and overall combustion judging from the pressure data. Meanwhile, the orifice diameter of 1.0 mm produces a higher jet velocity but a slower burn duration compared to the larger orifice diameter.

4.2 Experimental research

Experimental research on the pre-chamber ignition system can be divided into two types: the optical test and the thermal engine test. Optical tests on the combustion bomb, RCM, and optical engine mainly focus on the mechanisms and fundamental combustion. Thermo engine tests on single-cylinder and multi-cylinder engines are adopted to study the efficiency, emissions, engine tuning, and map-wide operation. A synthesis of those two different kinds of experimental methods is mandatory to explore the TJI design at the commercial level.

4.2.1 Optical test

With high-speed Schlieren measurements, optical tests are capable of visualizing the jet behaviors, ignition, and combustion evolution in the main chamber. Meanwhile, the active radicals in the jets are normally visualized with OH* Chemiluminescence, and the intensity of CH* is generally used to characterize the flame front. Those two species can be correlated with the local heat release [119]. However, measuring high-quality experimental data of the pre-chamber combustion is quite difficult considering its size and integration into the cylinder head. Even by adopting state-of-the-art optical techniques, some key physical and chemical phenomena are still not achievable.

Sens et al. [75] conducted optical tests in a high-pressure combustion cell, aiming at comparing the combustion processes with the conventional spark ignition and the passive pre-chamber ignition. With methane-air selected as the combustion mixture, the ignition pressure and temperature were controlled at 10 bar and 400 K, respectively, which correspond to the working condition of a typical engine operating at the load point of 6 bar BMEP @1500 rpm. The morphological image analysis indicated that the entrainment of high-turbulent ejected jets enables rapid growth of the flame area in the early combustion stage inside the main chamber, and the calculated flame speed is up to six times higher than that with the conventional spark plug. To investigate the effect of the excess air ratio on the flame behavior, Ju et al. [120] compared the open chamber and pre-chamber in a large bore constant volume chamber burning with methane/air mixtures. Optical results showed that the pre-chamber ignition can significantly increase the flame speed by 5~6 times under lean and stoichiometric conditions, compared to the maximum of 2.8 times under rich fuel combustion conditions.

To the best of the authors' knowledge, only Kyrtatos et al. [67] built an optical constant volume vessel equipped with an optically accessible pre-chamber in the open literature. The schematic of the corresponding optical pre-chamber is shown in Fig. 17, and the obtained Schlieren images (green/black) with superimposed OH* (pink) are illustrated in Fig. 18. The nozzle diameter for case 1 is fixed at 4 mm, compared to the 2 mm for case 2 and case 3. While, case 3 has an initial charge temperature of 430 K, which is higher than the initial temperature of 300 K in case 1 and case 2. In case 1, the OH* signal observed around the nozzle exit indicates that quenching within the nozzle is not complete. The hot products downstream of the nozzle further mix sufficiently with the cold unburned gasses, which suggests the flame quenching due to mixing. This is also verified with the tip of jets showing no OH* signal. In case 2 and case 3, the jet velocity is high due to the small orifice diameter, and complete quenching is observed either inside the nozzle or directly at the exit. Compared to case 2, the re-ignition in Case 3 is faster, which suggests the effect of initial temperature on the re-ignition propensity.

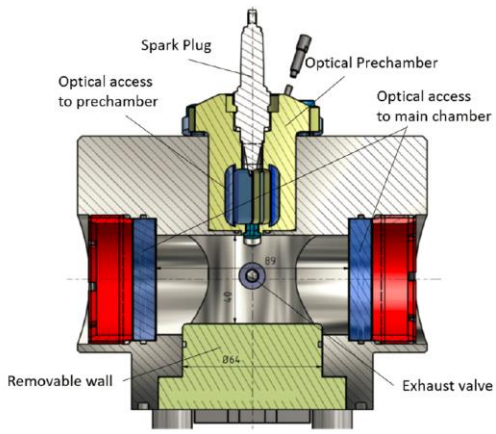

Figure 17. Schematic of the optical pre-chamber [67].

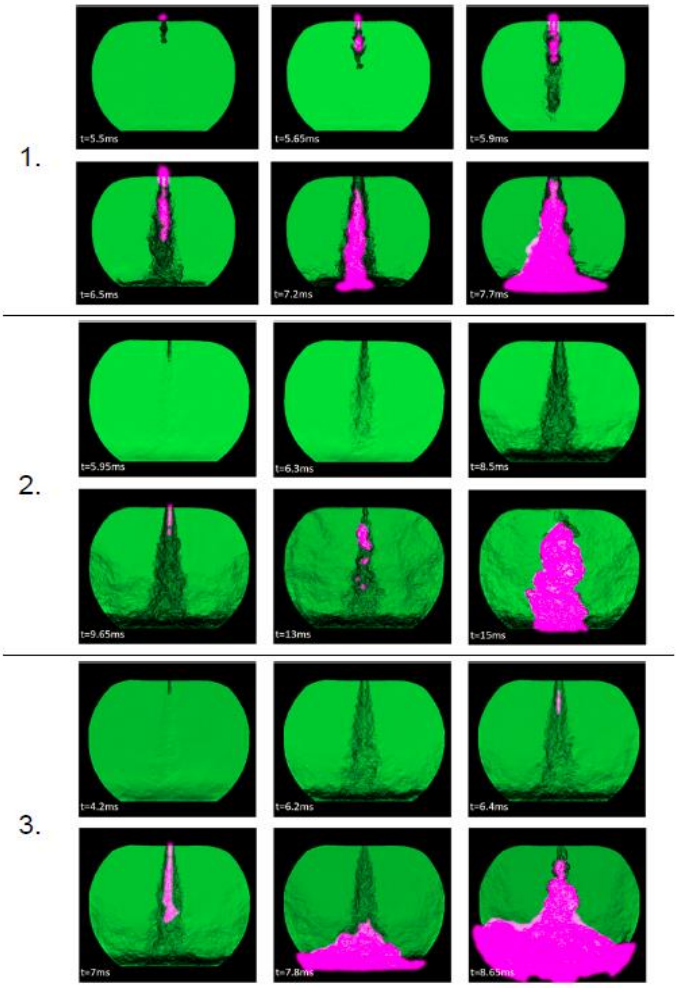

Figure 18. Schlieren images (green/black) and superimposed OH (pink) in the main chamber with three cases of different nozzle diameters and initial charge temperatures [67].*

Apart from the constant combustion cell, many optical studies on TJI systems were conducted on the RCM or the RCEM [121]. Desantes et al. [43] investigated an active pre-chamber ignition system operating at lean conditions with a RCEM. The high levels of turbulence and entrainment of fresh charge at jet surfaces are observed with Schlieren measurements. To evaluate the effects of the nozzle diameter and the configuration on the TJI ignition process, Gentz et al. [73, 122] conducted experiments of combustion visualization in a RCM burning with a premixed propane/air mixture. Optical images indicated that OH* and CH* radicals overlap spatially throughout the jet structure, and a faster and more vigorous jet is mandatory to ignite the leaner mixture. Meanwhile, the Reynolds number of the discharging jet is not sensitive to the nozzle diameter at the leaner condition of lambda=1.25.

Based on a well-established RCM, Thelen and Toulson [39] evaluated the effect of the orifice diameter ranging from 1.0 mm to 3.0 mm on combustion behavior. The pre-chamber, which connects to the main chamber by a nozzle containing a single orifice, has a volume of around 2% of that in the main chamber. It was found that the orifice size of 1.5 mm produces the fastest combustion rate, considering the trade-off between the positive turbulent effect and the negative restrictive loss generated by the nozzle orifice. Thelen and Toulson [38] further compared four different spark ignition locations in the pre-chamber. The result indicated that the location furthest from the bottoming orifice produces better main chamber ignition since more pre-chamber fuel is burned before the flame reaches the orifice to generate a high jet velocity in the main chamber.

Macián et al. [123] studied a stratified pre-chamber ignition system installed on a rapid compression-expansion machine. A zero-dimensional model is also developed to compute the instantaneous heat release rate in the pre-chamber with full considerations of the mass exchange between two chambers, heat transfer losses across walls, and turbulence intensity. Comparative results showed that the predicted flame speed agrees well with the averaged propagation speed obtained from broadband chemiluminescence visualization tests. Meanwhile, a decrease of 40% in the flame speed is observed with the equivalence ratio in the pre-chamber decreasing from slightly rich (fuel/air ratio of 1.1) to lean operation (fuel/air ratio of 0.9).

Tests conducted on optical single-cylinder engines can provide more fundamental engine like conclusions. Aiming at investigating the engine stability and efficiency in lean-burn operating conditions, Sementa et al. [124] compared the standard spark plug and the pre-chamber ignition configuration on an optical methane-fueled single-cylinder engine. Significant details of the flame propagation like the flame radius and flame speed were obtained. The results indicated that the flame speed with pre-chamber ignition is many times faster compared to the conventional SI engine, and the flame cycle to cycle variability also strongly decreases with the adoption of the pre-chamber ignition system.

With a modified optical single-cylinder egnine based on a 6-cylinder commercial heavy-duty engine, Sampath et al. [125] conducted simultaneous measurements of pressure traces, OH* chemiluminescence, and planar laser-induced fluorescence of acetone seeded in the main chamber. Comparisons of two different fueling ratios of 7% and 13% indicated that the increased fueling ratio leads to a phase lag in the pre-chamber jet penetration distance. This in turn delays the increase in the total OH* chemiluminescence intensity. However, the effect on the heat release rate seems much smaller since it is dominated by the global λ level.

Experiments on an optical engine emulating existing production designs were conducted by Bunce et al. [60] with special focuses on the interaction between the pre-chamber and main chamber events. As have been illustrated in Fig. 5, the reactive jets first appear in the main chamber are luminous. The visible jet formation first occurs approximately at the point of peak pre-chamber pressure. This is generally true for different pre-chamber designs. However, this luminosity quickly dissipates due to the sudden drop in temperature and pressure. Also, the entrainment of fresh charge contributes to the dilution of the visible jets. From 5 CAD before TDC, the jets turn to distinct and distributed ignition sites in the main chamber, followed by a rapid main chamber combustion event.

By synthesizing the optical and metal engine test results, Bunce et al. [60] indicated that although the jets enter the main chamber at a similar velocity with similar degrees of penetration and reactivity, conditions in the optical engine are less favorable for the main chamber combustion compared to the metal engine case. This is mainly because the operating condition in an optical engine differs from that of a real metal engine. Due to the nature of optical components, skip-fire strategies are normally adopted to control component temperatures. Also, the turbulence level inside an optical machine is expected to be different from that in a metal engine [62, 63, 126]. Thus, conclusions drawn from those studies might be restricted to particular engines and not generically applicable.

4.2.2 Thermo engine test

The single-cylinder test bench is flexible in evaluating the pre-chamber from aspects of combustion stability, lean limit level, and emissions. A multi-cylinder engine test could address thermal conditions and air management challenges of the final commercial application. Thus, it is essential to translate the single-cylinder test result into a multi-cylinder engine.

As the pre-chamber is normally designed without any change of the main chamber and cylinder header, a lightly lower CR is expected compared to the original SI engine. The increased heat transfer loss through chamber walls is another drawback of the pre-chamber ignition system. Theoretically, this increased heat loss can be attributed to the increased wall heat losses arising from the additional surface of the pre-chamber itself and the additional turbulence near the walls of the main combustion chamber. Sens et al. [5, 75] tried to distinguish those two types of heat loss at different operating conditions. The results indicated that the additional heat losses at part loads mainly result from the additional pre-chamber surface. On the contrary, the heat transfer loss through the main chamber occupies a large proportion of the additional heat losses at high engine loads. This is primarily because the intensified flame jets significantly increase local turbulence close to cylinder walls. Therefore, the trade-off between the local turbulence and knock mitigation potential should be seriously handled during the pre-chamber design.

Based on a single-cylinder engine adopted with an active gasoline-fueled pre-chamber, Stadler et al. [33] plotted a contour map of the indicated efficiency depending on air-fuel ratio and pre-chamber fuel mass ratio with the engine operating at the IMEP of 6 bar @ 1500 rpm. As shown in Fig. 19, a minimum pre-chamber mass ratio of 2% is mandatory to enable steady combustion at the air-fuel ratio up to 1.8. Meanwhile, the mass ratio of 5% looks to be the optimal value for engine efficiency. Further increasing the air-fuel ratio beyond 2.0 leads to a significant increase of unburnt HC, which restricts the increase of engine efficiency. It is concluded that the pre-chamber fueling does not influence the main combustion directly but mainly aims at ensuring a steady ignition in the main chamber.

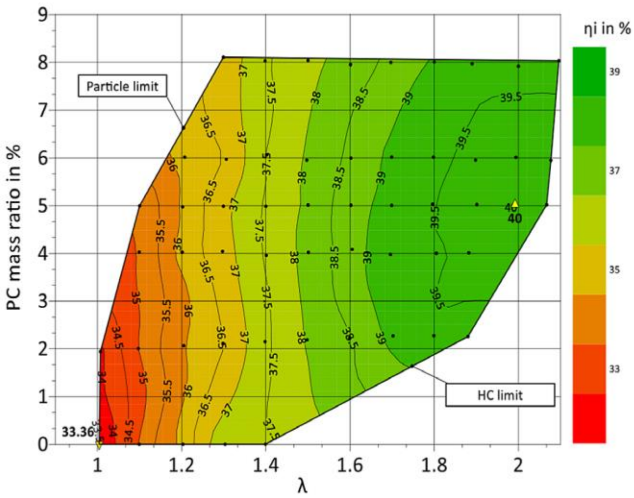

Figure 19. Contour map of the indicated efficiency map at IMEP of 6 bar @ 1500 rpm [33].

Considering the lower combustion temperature and longer burn duration under lean-burn conditions, combustion efficiency is assumed to decrease with the increasing lambda due to the influence of flame-wall interactions and crevice volume fuel [50]. Thus, the deteriorated combustion efficiency compromises the benefit arising from the decreased heat transfer loss. This will result in a peak thermal efficiency at a specific lambda value. It is also noted that the benefits of fuel consumption with the pre-chamber ignition system could not be fully achieved without any other tuning strategy. With test results over a load sweep from 6 bar up to 18 bar BMEP, Cooper et al. [74] confirmed that the reduced burn duration and improved combustion stability with the passive TJI could only translate into fuel economy benefit at high loads where engine knock limits the spark timing. At low loads below 14 bar BMEP, the fuel consumption with the passive TJI is slightly higher compared to the conventional SI engine. This is mainly because the increased heat losses cannot be fully compensated. Thus, other techniques like increasing the geometric CR should be adopted.

Bunce et al. [42, 76] compared the efficiency loss pathways in the baseline SI engine with those of the active TJI variant from lambda 1 to the lean limit. The compression ratios of the base SI engine and the TJI engine are fixed at 9:1 and 14:1, respectively. As shown in Fig. 20, the increased CR leads to a decrease in brake power at lambda 1 operation. This is mainly caused by the additional heat loss, due to the high mean gas temperature arising from the increased CR, and the retarded combustion phasing to avoid knock. It should be noted that the incomplete combustion loss of TJI is smaller compared to its counterpart in the SI engine, even a retarded combustion center by over 20 CAD is mandatory. At the lambda of 1.6, the combustion loss of TJI is equivalent to the base engine at stoichiometric conditions. The TJI combined with an increased CR leads to a brake thermal efficiency of nearly 42% at the lambda of 1.9, which represents an increase of thermal efficiency of over 19% compared to the SI engine. Stadler et al. [33] compared the SI, passive, and active pre-chamber configurations with or without an increased CR. It is concluded that the increased CR accompanied by the retard combustion leads to a deteriorated efficiency. While the passive pre-chamber mitigates the combustion knock but the larger heat losses prevent the efficiency from increasing. Lean burn with lambda of 2 increases efficiency by +2.5% compared to the conventional SI operation, and the fuel economy is increased by +5.4% with the increased compression ratio.

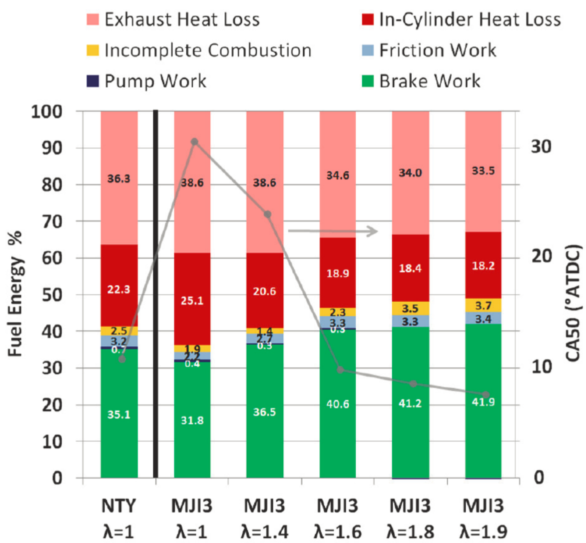

Figure 20. Comparison of efficiency loss pathways between the SI (NTY) and TJI (MJI3) at a knock limited condition (12 bar BMEP @ 3000 rpm) [42].

To make the sole gasoline jet ignition concept more robust and feasible over the wide speed and load domain, some other strategies are proposed. Schumacher et al. [127, 128] used the gasoline-vapor-air-mixture as active fueling. This gaseous mixture contains volatile fuel obtained in the fuel tank above the liquid surface. Controlled by a solenoid valve, the compressed and dosed mixture is injected into the pre-chamber. In addition, this new configuration can be easily modified to inject air additionally to the gasoline-vapor-air mixture. Thus, the pre-chamber can be actively purged, which increases combustion stability, especially at a high EGR rate. Attard et al. [82] proposed that a heated vaporized gasoline fuel is a good replacement for the liquid gasoline for the pre-chamber. Experimental results showed that the vaporized gasoline jet ignition system shows the highest lean lambda of up to 2.12 at 5% CoV IMEPg, compared to the value of 2.07 for the dual fuel and 1.94 for the liquid-fueled case. It is also concluded that the vaporized gasoline is a good substitute for the gaseous propane in fueling the pre-chamber. In addition, reduced spark plug fouling is confirmed with the vaporized gasoline-fueled pre-chamber [82].

4.3 Combinations with EGR or Miller cycle

In contrast to the conventional SI system, the pre-chamber ignition featured with distributed ignition sites is capable of complementing combustion processes with other fuel-saving technologies that decelerate combustion or turbulence. Thus, synergistic effects of the pre-chamber jet ignition concept with promising techniques like cooled external exhaust gas recirculation and Miller cycle should be investigated.

4.3.1 EGR

Similar to the lean-burn concept which dilutes the air-fuel mixture with fresh air, the EGR method diluting the cylinder charge with residual gas could increase the engine thermal efficiency effectively. Meanwhile, a deterioration in flammability and a decrease in the laminar flame speed is expected. In a conventional SI engine, typical flames, which are featured with moderate Reynolds numbers ($10<Re<100$) and Karlovitz numbers close or below 1, normally fall into the corrugated flamelets regime in a Borghi-Peters diagram [90, 129]. Assuming that the turbulence intensity and the integral length scale do not vary with the increase of the dilution rate, Benajes et al. [90] stated that the exhaust gas dilution, which effectively decreases the laminar flame speed and increases the flame thickness, can move the main chamber combustion into a more unstable regime in the Borghi-Peters diagrams. It is also noted that the EGR dilution is compatible with the three-way catalyst for NO_x control, which makes it more attractive when applied on the traditional SI engine.

Novella et al. [49] compared the air dilution and the EGR dilution with different passive pre-chamber designs. As shown in Fig. 21, the EGR dilution shows significantly different characteristics compared to the air dilution. Performances of the EGR dilution is more sensitive to the pre-chamber design. The maximum EGR dilution level is largely dependent on the pre-chamber geometry considering the trapped residual gases inside the pre-chamber. Cases of PC1 and PC2 with larger A/V ratios are preferred to ensure a good scavenging efficiency. Besides, none of the pre-chamber designs reach the EGR dilution limit of 30% obtained with the conventional SI concept, since the passive pre-chamber must cope with a residual gas rate higher than the main chamber average. This also means the turbulence and stratification inside the pre-chamber do not contribute to promoting the ignition and flame propagation process. Thus, spatial-temporal distributions of the residual gases, turbulence intensity, and flow velocity should be checked during the pre-chamber design.

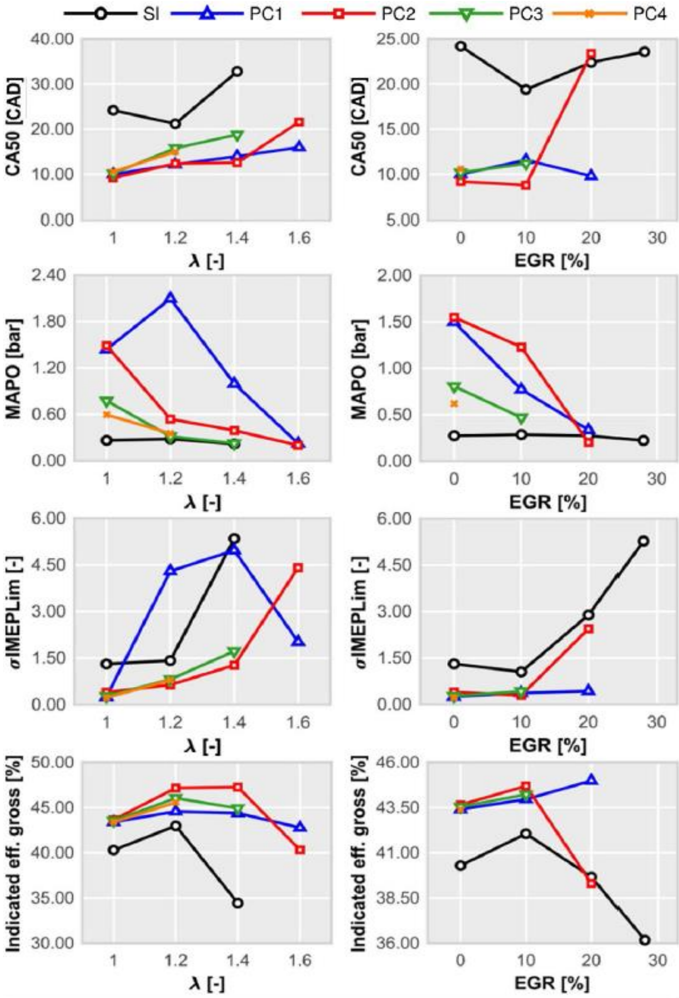

Figure 21. Comparisons of air dilution and EGR dilution at high load/speed conditions [49].

Sens et al. [5, 75] evaluated synergies of externally cooled EGR with both passive and active pre-chamber configurations. At knock-limited high loads, the passive pre-chamber with advanced combustion phasing leads to more stable combustion and thus increases the maximum EGR rate from the baseline value of 15% to 20%. At low loads, the EGR tolerance with passive pre-chamber is 5% points less than that of the conventional spark plug. This is mainly attributed to a large amount of residual gas trapped inside the main chamber and the deteriorated scavenging across the pre-chamber. Sens et al. [5, 75] also proposed a special active configuration with a premixed air/fuel mixture injected into the pre-chamber. Those two fluids are mixed directly before injection, and the prepared mixture can be supplied to the pre-chamber with any air/fuel ratio. Thus, the EGR compatibility can be significantly improved compared to the passive configuration but also to the active configuration with pure fuel injection. The maximum EGR rate of 31% was testified with experimental data obtained at BMEP of 16 bar @ 2000 rpm, compared to the maximum EGR rate of 15% with the conventional spark-ignited engine. However, external components and parasitic losses should be addressed.

4.3.2 Miller cycle

The Miller cycle normally achieved with late or early intake valve close strategy is featured with a reduced effective compression ratio. Further combined with an improved boosting system and external charge cooling, the Miller cycle can effectively reduce the cylinder temperature at the end of the compression stroke. Thus, the Miller cycle is treated as a competing technology to the externally cooled EGR, which is capable of improving both low-load operations with reduced pumping losses and wall heat losses and high-load operations because of its knock mitigation effect.

In general, the early intake valve closing (EIVC) is more preferred compared to the late intake valve closing (LIVC) based on the mechanical feasibility [75]. However, the charge motion decreases with the reduced valve lift. This leads to less combustion-promoting TKE and increased burn duration and burn delay. Sens et al. [75] plotted the averaged TKE levels in the cylinder and around the pre-chamber spark gap with standard and Miller camshafts. As shown in Fig. 22, the reduced charge motion with EIVC leads to a reduction of the turbulence level, and the cylinder TKE level is almost halved at the ignition timing. However, the TKE within the pre-chamber spark gap is mainly determined by the geometrical design of the pre-chamber and the engine operating load but is not affected by the Miller cycle. Sens et al. [75] also mentioned that the increased burn delay is mainly determined by the increased residual gas distribution and stoichiometric air-fuel ratio.

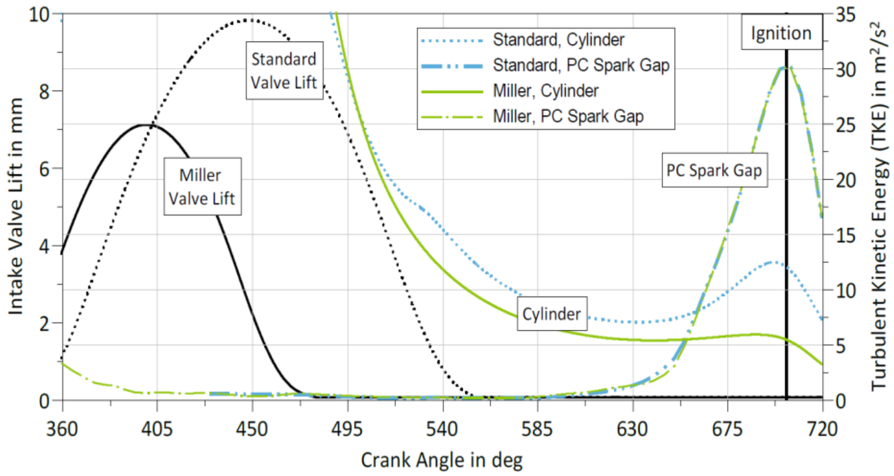

Figure 22. Comparisons of averaged turbulent kinetic energy levels in the cylinder and around the pre-chamber spark gap with standard and Miller camshafts at the BMEP of 4 bar @ 1250 rpm [75].

To evaluate the synergistic effect of the Miller cycle and pre-chamber ignition, experiments on a 1.5L variant of the DI3 engine operating at 3000 rpm under stoichiometric conditions were conducted by Cooper et al. [74]. Case sweeps with an increased geometric CR (from the base value of 9.25:1 to 14.7:1), a passive pre-chamber ignition system, and Miller cam profiles with durations of 152, 172, 246 (base engine) 292, 312 CAD were conducted. The results showed that compared to the LIVC counterparts, the EIVC cam profiles show better fuel economy due to their relatively better charge cooling effects and more homogenous mixing. The further inclusion of an external EGR strategy, meant that an optimal combustion phasing of 8 CAD after TDC can be achieved.

5 Critical issues of pre-chamber combustion systems

Although the TJI system has been testified on experimental prototypes, some critical issues still need to be fully addressed, like the hardware design and integration on existing cylinder heads, achieving acceptable combustion stability at low loads including idle and catalyst light-off, enabling whole-map operation, and lean aftertreatment for the active configuration. Without solving those limitations and critical issues, the benefits of jet ignition at part and high loads cannot be practically translated to non- and mild-hybrid engine applications.

5.1 Hardware design and integration

The TJI is designed to replace the typical central-mounted spark plug. The production-level durability is normally beyond the scope of most researches. Generally, there is no additional cooling arrangement in the cylinder head for the pre-chamber. When it comes to high speed and high load, temperatures of pre-chamber components could be very high, especially the pre-chamber cap and the spark plug electrodes. Thus, keeping component temperatures low to prevent irregular combustion like pre-ignition and glow ignition should be seriously handled. On the contrary, the excessive heat transfer losses through the pre-chamber walls are unfavorable for the combustion process at cold start and cold conditions.

The material choice for the pre-chamber is very important. Sens [75] et al. indicated that the high thermal conductivity materials such as low-alloy aluminum or copper could result in a significantly low surface temperature at high engine loads, which is far from the critical glow ignition condition. However, the surface temperature at low loads might fall into the flame extinction zone. Selecting steel as the pre-chamber material, elevated the surface temperature level at low loads reducing the flame extinction potential, but glow ignition might occur at high loads. Thus, to reduce the wall heat losses across the pre-chamber, the thermal conductivity of the material should be as small as possible without any glow ignition potential.

Design criteria of pre-chamber fuel injectors include micro-flow, minimal space claim, and low soot generation. As commercial direct injectors are not capable of metering very small quantities of liquid fuel for the pre-chamber, Attard and Blaxill [80] modified a production-based solenoid direct injector to fulfill the pre-chamber fuel flow requirements. The modifications included significantly reducing the injection pressure and changing the injector nozzle tip. Bench testing indicated that the modified injector hardware shows a far from optimal spray plume to cover the full operating envelope. Besides, rapid injector clogging appears to be one of the major technical challenges of metal engine testing. Analysis of the injector samples indicated that the likely cause of the coking is the external combustion exacerbated by the injector nozzle holes that are much smaller than those of production injectors.

5.2 Low load and cold start

Although the high load thermal performance is most relevant to CO_2 emissions from a hybrid powertrain, low load and idle operation conditions should be kept in mind. The potential weakness of the pre-chamber under low load conditions is attributed to the poor combustion stability at heavily throttled low loads and poor spark retard capability at loads consistent with idle and cold start spark retard (CSSR) catalyst heating operation. In general, the passive TJI system suffers more from issues of comparable idle and spark retard capability. On the contrary, the active TJI providing more control over the pre-chamber mixture preparation offers the flexibility to mitigate the deteriorated scavenging and poor combustion stability under heavily throttled operation and CSSR conditions.

At a high load, the strong scavenging across the pre-chamber leads to intense flame jets. However, the jets are very weak at low loads. With a cold engine, the heat released inside the pre-chamber is dissipated via the cold walls. Thus, those hot jets are further cooled down when mixing with the gases in the main chamber, which makes the ignition in the main chamber more difficult. By adapting the overflow geometry or spark gap location and by means of separately heating, such as an integrated electric heating coil, the heat dissipation and jet dilution under low load can be improved. IAV [5] proved that the heated pre-chamber can successfully address the engine cold start issues. Meanwhile, Mahle [42] stated that the patented TJI components could provide a degree of freedom for achieving a cold start.

To heat the catalytic converter after the engine cold-start, a later heat release rate is required. In general, very late combustion with acceptable combustion stability, i.e. combustion center of 75 deg crank angle after TDC, is adopted during catalyst heating operation in a conventional SI engine [75]. This unfavorable ignition condition brings more challenges to the pre-chamber during cold conditions. Mahle [42, 74] indicated that those issues can be addressed by optimizing the pre-chamber geometric parameters like shape, volume, and nozzle diameter, and successful utilization of both passive and active pre-camber configurations at low load and CSSR strategies were investigated. However, this optimized geometry in turn will slightly deteriorate the knock advantage and fuel benefits. Sens et al. [75] compared two different pre-chamber layouts shown in Fig. 23. The pre-chamber with configuration A, which was designed for high knock benefit and fuel consumption reduction at part load, could provide the best efficiency when the combustion center is around 8 deg crank angle after TDC. This can be verified with the clear central and lateral flame jets observed in the main chamber. However, it could only tolerate the maximum delay of the combustion center to 25 deg crank angle after TDC. With an updated layout B equipped with a much larger central bore, the combustion center can be retarded to 46 deg crank angle after TDC, as the central jets still persist.

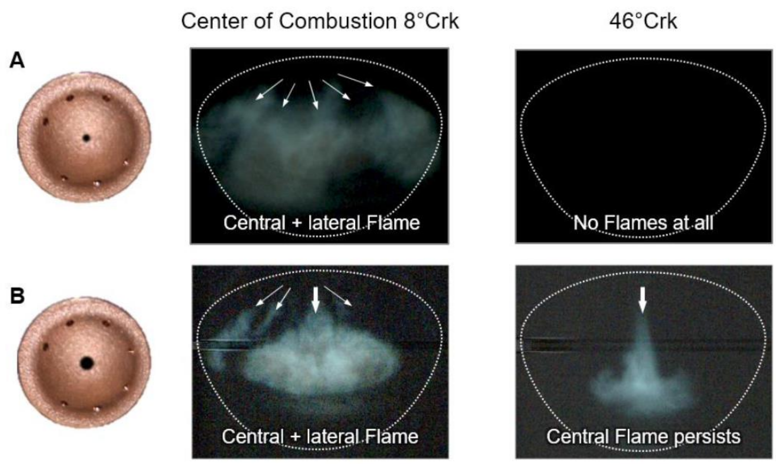

Figure 23. Optical images of two different pre-chamber layouts adopted on a single-cylinder engine operating at the BMEP of 2 bar @ 1250 rpm [75].

It is known that the state-of-the-art three-way catalysts are not compatible with the lean burn concept. Active pre-chamber ignition systems operating under lean conditions necessitate the use of lean aftertreatment. Internal studies conducted by Mahle [42, 130] indicated that the use of commercially available diesel passenger car aftertreatment systems can result in compliance with US emissions regulations.

5.3 Cost and techno economy

The TJI engine is built by replacing the conventional spark plug with a pre-chamber. With respect to the passive TJI system, the stoichiometric operation allows the adoption of the three-way catalyst for emission control. Thus, the passive TJI is featured with a low cost and engineering straightforwardness. Regarding the active TJI system, an additional fuel injection system that can handle a very small fuel mass flow rate precisely is mandatory. Meanwhile, the lean operation requires the use of lean aftertreatment or oxidation catalyst. Therefore, the cost of the active TJI system would be higher than that of the passive TJI which has a similar cost as the conventional SI engine. Since the TJI technology has been limited to research laboratories, its techno economy is seldomly reported. Concerning the long-term fleet target of reducing CO_2 emissions from future light-duty vehicles, the initial TJI penetration is more likely to occur on the hybrid powertrain rather than the conventional thermal engine.

5.4 Integration of TJI with artificial intelligence

The application of artificial intelligence in applied engine studies is mainly emulating the modeling results from 1D and 3D CFD simulations [1–7]. Taghavifar et al. [131] trained a support vector machine using CFD simulations to obtain the optimized chamber geometry of a diesel engine. Moiz et al. [132] integrated machine learning into a genetic algorithm, which optimizes the operating conditions of a heavy-duty diesel engine. The learning model comes from a group of different machine learning algorithms and was trained CFD simulations conducted on a supercomputer. The prediction of knock onset based on a supervised deep-learning algorithm was carried out by Cho et al. [133] using data from CFD simulations, while Petrucci et al. [134] applied three machine learning methods for knock onset prediction with data from 1D engine simulations. Badra et al. [135] developed a Machine Learning-Grid Gradient

Ascent approach which was used to optimize the operating conditions and the piston bowl design for combustion engines. Although these works provided approaches to incorporate artificial intelligence into the engine studies, they were not focused on the pre-chamber SI engine. Only a recent study by Posch et al. [136] applied an artificial neural network to emulate the results from simplified CFD simulations of the pre-chamber SI engine, which relatively well reproduces the overall trends of output parameters. Therefore, the application of artificial intelligence in pre-chamber SI engine shows great potential but still needs to be further developed.

6 Conclusions and future research directions

6.1 Conclusions

This paper presents a comprehensive review of the pre-chamber ignition system applied on future low-carbon spark ignition engines. After detailed discussions on operating mechanisms, design criteria, comparative numerical and experimental studies, state-of-the-art development, and critical issues for future commercialization, the following conclusions are obtained.

1) The scavenging and filling across the pre-chamber are mainly controlled by the piston moving and the additional fueling if applicable. The jet penetration prior to ignition determines the ignition site distributions, and the flame quenching phenomenon distinguishes the TJI from the conventional pre-chamber ignition systems. The combustion in the main chamber is controlled by the thermal, chemical, and turbulent effects of the jets.

2) In the pre-chamber design, the jet penetration should be controlled to minimize the distance each flame front traveling to consume the charge. Among those geometrical parameters, the orifice diameter plays the most significant role in determining the scavenging process, flame quenching, and jet velocity. A fully optimized pre-chamber configuration incorporates multiple criteria including operating strategies, boost requirements, compression ratio, catalyst heating, and cost-benefit.

3) As a low-cost technology, the passive TJI system operating under the stoichiometric condition enables fast and stable combustion, high compression ratio

operation, and the utilization of conventional after-treatment, and the fuel consumption is assumed to be improved by 2 to 3% in the driving-cycle relevant area. Featured with the high cost and complex components, the active TJI system operating under the lean-burn condition with the lambda up to 2 enables high efficiency and low NO_x emissions. Further combining with the cooled EGR, Miller cycle, and increased compression ratio, a maximum indicated thermal efficiency of 47% is achievable.

6.2 Future research directions

Potential knowledge gaps for future research are identified as follows. The fluid-mechanical and chemical-kinetic processes governing the pre-chamber and main chamber ignition and combustion are still not fully exploited. Fundamental studies on providing insights into the spatial ignition and self-generated turbulence and identifying the flame regime under TJI combustion are highly recommended for future research. Concerning the pre-chamber design, relationships between geometrical parameters and physical jet properties including velocity, penetration prior to ignition, and ignition site distribution should be further evaluated. Furthermore, the lack of predictive models for jet ignition and combustion places obstacles in the way of pre-chamber design and optimization. Finally, operation strategies of the pre-chamber ignition system in conjunction with other complementary technologies adopted on different future powertrains need to be clarified.

Acknowledgment

This work was supported by the National Natural Science Foundation of China (No. 51809166) and the “Advance Propulsion Centre – APC5”.

Reference

[1] Joshi A. Review of vehicle engine efficiency and emissions. SAE Technical Paper 2020-01-0352; 2020.

[2] Reitz R, Ogawa H, Payri R, Fansler T, Kokjohn S, Moriyoshi Y, et al. IJER editorial: The future of the internal combustion engine. SAGE Publications Sage UK: London, England; 2020.

[3] Leach F, Kalghatgi G, Stone R, Miles P. The scope for improving the efficiency and environmental impact of internal combustion engines. Transportation Engineering. 2020:100005.

[4] Ganesan V. Internal combustion engines: McGraw Hill Education (India) Pvt Ltd; 2012.

[5] Sens M, Binder E. Pre-chamber ignition as a key technology for future powertrain fleets. MTZ worldwide. 2019;80:44-51.

[6] Boretti A. Lean-burn stratified alcohol fuels engines of power density up to 475 kW/Liter featuring super-turbocharging, rotary valves, direct injection, and jet ignition. SAE Technical Paper 2020-01-2036; 2020.

[7] Lajunen A, Sainio P, Laurila L, Pippuri-Mäkeläinen J, Tammi K. Overview of powertrain electrification and future scenarios for non-road mobile machinery. Energies. 2018;11:1184.

[8] Sens M, Günther M, Medicke M, Walther U. Developing a spark-ignition engine with 45% efficiency. MTZ worldwide. 2020;81:46-51.

[9] Sellnau M, Foster M, Moore W, Sinnamon J, Hoyer K, Klemm W. Pathway to 50% brake thermal efficiency using gasoline direct injection compression ignition. SAE International Journal of Advances and Current Practices in Mobility. 2019;1:1581-603.

[10] Wang Z, Liu H, Reitz RD. Knocking combustion in spark-ignition engines. Progress in Energy and Combustion Science. 2017;61:78-112.

[11] Zhen X, Wang Y, Xu S, Zhu Y, Tao C, Xu T, et al. The engine knock analysis–An overview. Applied Energy. 2012;92:628-36.

[12] Serrano D, Zaccardi J-M, Müller C, Libert C, Habermann K. Ultra-lean pre-chamber gasoline engine for future hybrid powertrains. SAE International Journal of Advances and Current Practices in Mobility. 2019;2:607-22.

[13] Tang Q, Liu J, Zhan Z, Hu T. Influences on combustion characteristics and performances of EGR vs. lean burn in a gasoline engine. SAE Technical Paper 2013-01-1125; 2013.

[14] Scarcelli R, Matthias N, Wallner T. Numerical investigation of combustion in a lean burn gasoline engine. SAE Technical Paper 2013-24-0029; 2013.

[15] Burrows J, Lykowski J, Mixell K. Corona ignition system for highly efficient gasoline engines. MTZ worldwide. 2013;74:38-41.

[16] Silva S, Grimaldi A, Carugati E, Merola SS, Irimescu A, Valentino G, et al. Experimental evaluation of an advanced ignition system for GDI engines. SAE International Journal of Engines. 2015;8:2351-67.

[17] Briggs T, Alger T, Mangold B. Advanced ignition systems evaluations for high-dilution SI engines. SAE International Journal of Engines. 2014;7:1802-7.

[18] Müller C, Morcinkowski B, Schernus C, Habermann K, Uhlmann T. Development of a pre-chamber for spark ignition engines in vehicle applications. Ignition Systems for Gasoline Engines: 4th International Conference, December 6-7, 2018, Berlin, Germany Ed: M Günther2018. p. 261.

[19] Dale J, Oppenheim A. Enhanced ignition for IC engines with premixed gases. SAE Transactions 810146. 1981:606-21.

[20] Dale JD, Checkel M, Smy P. Application of high energy ignition systems to engines. Progress in energy and combustion science. 1997;23:379-98.

[21] Yun H, Idicheria C, Najt P. The effect of advanced ignition system on gasoline low temperature combustion. International Journal of Engine Research. 2019;22:417-29.

[22] Jamrozik A. Lean combustion by a pre-chamber charge stratification in a stationary spark ignited engine. Journal of Mechanical Science and Technology. 2015;29:2269-78.

[23] Toulson E, Schock HJ, Attard WP. A review of pre-chamber initiated jet ignition combustion systems. SAE Technical Paper 2010-01-2263; 2010.

[24] Toulson E, Watson HC, Attard WP. Gas assisted jet ignition of ultra-lean LPG in a spark

ignition engine. SAE Technical Paper 2009-01-0506; 2009.

[25] Alvarez CEC, Couto GE, Roso VR, Thiriet AB, Valle RM. A review of prechamber ignition systems as lean combustion technology for SI engines. Applied Thermal Engineering. 2018;128:107-20.

[26] Turkish MC. 3-valve stratified charge engines: Evolvement, analysis and progression. SAE Transactions. 1974:3483-503.

[27] Oppenheim AK. Prospects for combustion in piston engines. SAE Transactions. 2002:1707-21.

[28] Yagi S, Dath T, Ukawa H, Fujii I. Research and development of honda cvcc engine. Paper C13/75 presented at IMechE Conference1976.

[29] Noguchi M, Sanda S, Nakamura N. Development of Toyota lean burn engine. SAE Transactions. 1976:2358-73.

[30] Adams TG. Torch ignition for combustion control of lean mixtures. SAE Technical Paper 790440; 1979.

[31] Brandstetter W. The volkswagen lean burn pc-engine concept. SAE Transactions. 1980:1804-21.

[32] Alvarez CEC, Roso VR, Santos NDSA, Fernandes AT, Valle RM. Combustion analysis in a SI engine with homogeneous and stratified pre-chamber system. SAE Technical Paper 2018-36-0112; 2018.

[33] Stadler A, Sauerland H, Härtl M, Wachtmeister G. The potential of gasoline fueled pre-chamber ignition combined with elevated compression ratio. SAE Technical Paper 2020-01-0279; 2020.

[34] Gussak L, Karpov V, Tikhonov YV. The application of lag-process in prechamber engines. SAE Transactions. 1979:2355-80.

[35] Telli GD, Altafini CR, Costa CA, Rosa JS, Martins ME, Oliveira Rocha LA. A comprehensive review of homogeneous charge compression ignition (HCCI) engines: Advantages, challenges and evolution. SAE Technical Paper 2020-36-0042; 2021.

[36] Agarwal AK, Singh AP, Maurya RK. Evolution, challenges and path forward for low temperature combustion engines. Progress in Energy and Combustion Science. 2017;61:1-56.

[37] Bendu H, Murugan S. Homogeneous charge compression ignition (HCCI) combustion: Mixture preparation and control strategies in diesel engines. Renewable and Sustainable Energy Reviews. 2014;38:732-46.

[38] Thelen BC, Toulson E. A computational study of the effects of spark location on the performance of a turbulent jet ignition system. SAE Technical Paper 2016-01-0608; 2016.

[39] Thelen BC, Toulson E. A computational study on the effect of the orifice size on the performance of a turbulent jet ignition system. Proceedings of the Institution of Mechanical Engineers, Part D: Journal of Automobile Engineering. 2017;231:536-54.

[40] Blankmeister M, Alp M, Shimizu E. Passive pre-chamber spark plug for future gasoline combustion systems with direct injection. Ignition Systems for Gasoline Engines: 4th International Conference, Berlin, Germany Ed: M Günther2018. p. 149.

[41] Benajes J, Novella R, Gomez-Soriano J, Barbery I, Libert C, Rampanarivo F, et al. Computational assessment towards understanding the energy conversion and combustion process of lean mixtures in passive pre-chamber ignited engines. Applied Thermal Engineering. 2020;178:115501.

[42] Bunce M, Blaxill H, Cooper A. Development of both active and passive pre-chamber jet ignition multi-cylinder demonstrator engines. 28th Aachen Colloquium Automobile and Engine Technology, Aachen2019. p. 907-42.

[43] Desantes JM, Novella R, De La Morena J. Achieving ultra-lean combustion using a pre-chamber spark ignition system in a rapid compression-expansion machine. SAE Technical Paper 2019-01-0236; 2019.

[44] Almatrafi F, Hlaing P, Marquez ME, Houidi MB, Johansson B. Narrow-throat pre-chamber combustion with ethanol, a comparison with methane. SAE Technical Paper 2020-01-2041; 2020.

[45] Attard W, Fraser N, Parsons P, Toulson E. A turbulent jet ignition pre-chamber combustion system for large fuel economy improvements in a modern vehicle powertrain. SAE Technical Paper 2010-01-1457; 2010.

[46] Liu F, Zhou L, Hua J, Liu C, Wei H. Effects of pre-chamber jet ignition on knock and combustion characteristics in a spark ignition engine fueled with kerosene. Fuel. 2021;293:120278.

[47] Novella R, Gomez-Soriano J, Martinez-Hernandiz PJ, Libert C, Rampanarivo F. Improving the performance of the passive pre-chamber ignition concept for spark-ignition engines fueled with natural gas. Fuel. 2021;290:119971.

[48] Gupta HN. Fundamentals of internal combustion engines: PHI Learning Pvt. Ltd.; 2012.

[49] Novella R, Pastor J, Gomez-Soriano J, Barbery I, Libert C, Rampanarivo F, et al. Experimental and numerical analysis of passive pre-chamber ignition with EGR and air dilution for future generation passenger car engines. SAE Technical Paper 2020-01-0238; 2020.

[50] Peters N, Subramanyam SKP, Bunce M, Blaxill H, Cooper A. Optimization of lambda across the engine map for the purpose of maximizing thermal efficiency of a jet ignition engine. SAE Technical Paper 2020-01-0278; 2020.

[51] Silva M, Sanal S, Hlaing P, Cenker E, Johansson B, Im HG. Effects of geometry on passive pre-chamber combustion characteristics. SAE Technical Paper 2020-01-0821; 2020.

[52] Distaso E, Amirante R, Cassone E, Catapano F, De Palma P, Sementa P, et al. Experimental and numerical analysis of a pre-chamber turbulent jet ignition combustion system. SAE Technical Paper 2019-24-0018; 2019.

[53] Distaso E, Amirante R, Cassone E, De Palma P, Sementa P, Tamburrano P, et al. Analysis of the combustion process in a lean-burning turbulent jet ignition engine fueled with methane. Energy Conversion and Management. 2020;223:113257.

[54] Bardis K, Xu G, Kyrtatos P, Wright YM, Boulouchos K. A zero dimensional turbulence and heat transfer phenomenological model for pre-chamber gas engines. SAE Technical Paper 2018-01-1453; 2018.

[55] Xu G, Wright YM, Schiliro M, Boulouchos K. Characterization of combustion in a gas engine ignited using a small un-scavenged pre-chamber. International Journal of Engine Research. 2020;21:1085-106.

[56] Xu G, Kotzagianni M, Kyrtatos P, Wright YM, Boulouchos K. Experimental and numerical investigations of the unscavenged prechamber combustion in a rapid compression and expansion machine under engine-like conditions. Combustion and Flame. 2019;204:68-84.

[57] Chinnathambi P, Bunce M, Cruff L. RANS based multidimensional modeling of an ultra-lean burn pre-chamber combustion system with auxiliary liquid gasoline injection. SAE Technical Paper 2015-01-0386; 2015.

[58] Rajasegar R, Niki Y, García-Oliver JM, Li Z, Musculus MPB. Fundamental insights on

ignition and combustion of natural gas in an active fueled pre-chamber spark-ignition system. Combustion and Flame. 2021;232:111561.

[59] Tang Q, Sampath R, Marquez ME, Sharma P, Hlaing P, Houidi MB, et al. Optical diagnostics on the pre-chamber jet and main chamber ignition in the active pre-chamber combustion (PCC). Combustion and Flame. 2021;228:218-35.

[60] Bunce M, Blaxill H, Kulatilaka W, Jiang N. The effects of turbulent jet characteristics on engine performance using a pre-chamber combustor. SAE Technical Paper 2014-01-1195; 2014.

[61] Biswas S, Qiao L. Ignition of ultra-lean premixed H2/air using multiple hot turbulent jets generated by pre-chamber combustion. Applied Thermal Engineering. 2018;132:102-14.

[62] Biswas S, Tanvir S, Wang H, Qiao L. On ignition mechanisms of premixed CH4/air and H2/air using a hot turbulent jet generated by pre-chamber combustion. Applied Thermal Engineering. 2016;106:925-37.

[63] Yamaguchi S, Ohiwa N, Hasegawa T. Ignition and burning process in a divided chamber bomb. Combustion and flame. 1985;59:177-87.

[64] Wöbke M, Reinicke P-B, Rieß M, Römer Lv, Sens M. Characterization of the ignition and early flame propagation of pre-chamber ignition system in a high pressure combustion cell. Ignition Systems for Gasoline Engines : 4th International Conference, December 6 - 7, 2018, Berlin, Germany Ed: M Günther: expert Verlag, Tübingen; 2018. p. 385-423.

[65] Gussak L. High chemical activity of incomplete combustion products and a method of prechamber torch ignition for avalanche activation of combustion in internal combustion engines. SAE Transactions. 1975:2421-45.

[66] Gussak L. The role of chemical activity and turbulence intensity in prechamber-torch organization of combustion of a stationary flow of a fuel-air mixture. SAE Technical Paper 830592; 1983.

[67] Kyrtatos P, Bardis K, Bolla M, Denisov A, Wright Y, Herrmann K, et al. Transferability of insights from fundamental investigations into practical applications of prechamber combustion systems. Ignition Systems for Gasoline Engines: Internationale Tagung Zündsysteme für Ottomotoren. 2018:442.

[68] Boust B, Sotton J, Labuda S, Bellenoue M. A thermal formulation for single-wall quenching of transient laminar flames. Combustion and flame. 2007;149:286-94.

[69] Muller M, Freeman C, Zhao P, Ge H. Numerical simulation of ignition mechanism in the main chamber of turbulent jet ignition system. Internal Combustion Engine Division Fall Technical Conference: American Society of Mechanical Engineers; 2018. p. V002T06A10.

[70] Tang W, Sarathy M. Investigate chemical effects of pre-chamber combustion products on main chamber ignition performance under an ultra-lean condition. SAE Technical Paper 2020-01-2001; 2020.

[71] Qin F, Shah A, Huang Z-w, Peng L-n, Tunestal P, Bai X-S. Detailed numerical simulation of transient mixing and combustion of premixed methane/air mixtures in a pre-chamber/main-chamber system relevant to internal combustion engines. Combustion and Flame. 2018;188:357-66.

[72] Korb B, Kuppa K, Nguyen HD, Dinkelacker F, Wachtmeister G. Experimental and numerical investigations of charge motion and combustion in lean-burn natural gas engines. Combustion and Flame. 2020;212:309-22.

[73] Gentz G, Thelen B, Litke P, Hoke J, Toulson E. Combustion visualization, performance,

and CFD modeling of a pre-chamber turbulent jet ignition system in a rapid compression machine. SAE International Journal of Engines. 2015;8:538-46.

[74] Cooper A, Harrington A, Bassett M, Reader S, Bunce M. Application of the passive MAHLE jet ignition system and synergies with Miller cycle and exhaust gas recirculation. SAE Technical Paper 2020-01-0283; 2020.

[75] Sens M, Binder E, Reinicke P, Riess M, Stappenbeck T, Woebke M. Pre-chamber ignition and promising complementary technologies. 27th Aachen Colloquium, Aachen2018.

[76] Peters N, Bunce M, Blaxill H. The impact of engine displacement on efficiency loss pathways in a highly dilute jet ignition engine. SAE Technical Paper 2019-01-0330; 2019.

[77] Hua J, Zhou L, Gao Q, Feng Z, Wei H. Effects on cycle-to-cycle variations and knocking combustion of turbulent jet ignition (TJI) with a small volume pre-chamber. SAE Technical Paper 2020-01-1119; 2020.

[78] Hua J, Zhou L, Gao Q, Feng Z, Wei H. Influence of pre-chamber structure and injection parameters on engine performance and combustion characteristics in a turbulent jet ignition (TJI) engine. Fuel. 2021;283:119236.

[79] Attard WP, Blaxill H, Anderson EK, Litke P. Knock limit extension with a gasoline fueled pre-chamber jet igniter in a modern vehicle powertrain. SAE International Journal of Engines. 2012;5:1201-15.

[80] Attard WP, Blaxill H. A single fuel pre-chamber jet ignition powertrain achieving high load, high efficiency and near zero NOx emissions. SAE International Journal of Engines. 2012;5:734-46.

[81] Sementa P, Catapano F, Di Iorio S, Vaglieco BM. Effects of prechamber on efficiency improvement and emissions reduction of a SI engine fuelled with gasoline. SAE Technical Paper 2019-24-0236; 2019.

[82] Attard WP, Blaxill H. A lean burn gasoline fueled pre-chamber jet ignition combustion system achieving high efficiency and low nox at part load. SAE Technical Paper 2012-01-1146; 2012.

[83] Atis C, Schock H. Comparison of excess air (lean) vs EGR diluted operation in a pre-chamber air/fuel scavenged dual mode, turbulent jet ignition engine at high dilution rate (~40%). SAE International Journal of Advances and Current Practices in Mobility. 2021;3:1569-84.

[84] Sementa P, Catapano F, Di Iorio S, Todino M, Vaglieco BM. Turbulent jet ignition effect on exhaust emission and efficiency of a SI small engine fueled with methane and gasoline. SAE Technical Paper 2020-24-0013; 2020.

[85] Bureshaid KI, Feng D, Bunce M, Zhao H. Experimental studies of gasoline auxiliary fueled turbulent jet igniter at different speeds in single cylinder engine. SAE Technical Paper 2019-24-0105; 2019.

[86] Joshi A. Review of vehicle engine efficiency and emissions. SAE Technical Paper 2020-01-0352; 2020.

[87] Hlaing P, Echeverri Marquez M, Shankar V, Cenker E, Ben Houidi M, Johansson B. A study of lean burn pre-chamber concept in a heavy duty engine. SAE Technical Paper 2019-24-0107. 2019.

[88] Baumgartner LS, Karmann S, Backes F, Stadler A, Wachtmeister G. Experimental investigation of orifice design effects on a methane fuelled prechamber gas engine for automotive applications. SAE Technical Paper 2017-24-0096; 2017.

[89] Attard WP, Toulson E, Huisjen A, Chen X, Zhu G, Schock H. Spark ignition and pre-chamber turbulent jet ignition combustion visualization. SAE Technical Paper 2012-01-0123; 2012.

[90] Benajes J, Novella R, Gómez-Soriano J, Martinez-Hernandiz PJ, Libert C, Dabiri M. Evaluation of the passive pre-chamber ignition concept for future high compression ratio turbocharged spark-ignition engines. Applied Energy. 2019;248:576-88.

[91] Bolla M, Shapiro E, Tiney N, Kyrtatos P, Kotzagianni M, Boulouchos K. Numerical study of turbulence and fuel-air mixing within a scavenged pre-chamber using RANS and LES. SAE Technical Paper 2019-01-0198; 2019.

[92] Wallesten J, Chomiak J. Investigation of spark position effects in a small pre-chamber on ignition and early flame propagation. SAE transactions. 2000:2477-85.

[93] Attard WP, Parsons P. Flame kernel development for a spark initiated pre-chamber combustion system capable of high load, high efficiency and near zero NOx emissions. SAE International Journal of Engines. 2010;3:408-27.

[94] Attard WP, Kohn J, Parsons P. Ignition energy development for a spark initiated combustion system capable of high load, high efficiency and near zero NOx emissions. SAE International Journal of Engines. 2010;3:481-96.

[95] Toulson E, Watson HC, Attard WP. The effects of hot and cool EGR with hydrogen assisted jet ignition. SAE Technical Paper 2007-01-3627; 2007.

[96] Attard WP, Blaxill H. A gasoline fueled pre-chamber jet ignition combustion system at unthrottled conditions. SAE International Journal of Engines. 2012;5:315-29.

[97] Hlaing P, Marquez ME, Singh E, Almatrafi F, Cenker E, Houidi MB, et al. Effect of pre-chamber enrichment on lean burn pre-chamber spark ignition combustion concept with a narrow-throat geometry. SAE Technical Paper 2020-01-0825; 2020.

[98] Attard WP, Parsons P. A normally aspirated spark initiated combustion system capable of high load, high efficiency and near zero NOx emissions in a modern vehicle powertrain. SAE International Journal of Engines. 2010;3:269-87.

[99] Gupta A, Sharma S, Narayan S. Gasoline Engine Technology: Combustion Engines: An Introduction to Their Design, Performance, and Selection; 2017.

[100] Marquez ME, Hlaing P, Tang Q, Sampath R, Cenker E, Houidi MB, et al. High-speed imaging of main-chamber combustion of a narrow throat pre-chamber under lean conditions. SAE Technical Paper 2020-01-2081; 2020.

[101] Tang Q, Sampath R, Marquez ME, Hlaing P, Sharma P, Ben M, et al. Simultaneous negative PLIF and OH* chemiluminescence imaging of the gas exchange and flame jet from a narrow throat pre-chamber. SAE Technical Paper 2020-01-2080; 2020.

[102] Bozza F, De Bellis V, Tufano D, Malfi E, Müller C, Habermann K. 1D numerical and experimental investigations of an ultralean pre-chamber engine. SAE International Journal of Engines. 2019;13:159-74.

[103] Bosi L, Ciampolini M, Romani L, Balduzzi F, Ferrara G. Experimental analysis on the effects of passive prechambers on a small 2-stroke low-pressure direct injection (LPDI) engine. SAE Technical Paper 2020-32-2305; 2020.

[104] Yu X, Zhang A, Baur A, Engineer N. The impact of pre-chamber design on part load efficiency and emissions of a Miller cycle light duty gasoline engine. SAE Technical Paper 2021-01-0479; 2021.

[105] Janas P, Niessner W. Towards a thermally robust automotive pre-chamber spark plug

for turbocharged direct injection gasoline engines. Ignition Systems for Gasoline Engines: 4th International Conference, December 6-7, 2018, Berlin, Germany Ed: M Günther2018. p. 122.

[106] Novella R, Pla B, Bares P, Martinez-Hernandiz PJ. Closed-Loop Combustion Control by Extremum Seeking with the Passive-Chamber Ignition Concept in SI Engines. SAE Technical Paper 2020-01-1142; 2020.

[107] Cruz IWSL, Alvarez CEC, Teixeira AF, Valle RM. Zero-dimensional mathematical model of the torch ignited engine. Applied Thermal Engineering. 2016;103:1237-50.

[108] Onofrio G, Li C, Valladolid PG, De La Morena J, Garcia A, Tunestal P, et al. Experimental and numerical asessment of active pre-chamber ignition in heavy duty natural gas stationary engine. SAE Technical Paper 2020-01-0819; 2020.

[109] Hiraoka K, Nomura K, Yuuki A, Oda Y, Kameyama T. Phenomenological 0 dimensional combustion model for spark-ignition natural gas engine equipped with pre-chamber. SAE Technical Paper 2016-01-0556; 2016.

[110] Kouremenos D, Rakopoulos C, Hountalas D. Thermodynamic analysis of indirect injection diesel engines by two-zone modeling of combustion. ASME J Eng Gas Turbines Power January 1990; 112(1): 138–149. 1990.

[111] Bozza F, De Bellis V, Tufano D, Malfi E, Müller C, Habermann K. A quasi-dimensional model of pre-chamber spark-ignition engines. SAE Technical Paper 2019-01-0470; 2019.

[112] De Bellis V, Malfi E, Bozza F, KUMAR D, Serrano D, Dulbecco A, et al. Experimental and 0D numerical investigation of ultra-lean combustion concept to improve the efficiency of SI engine. SAE International Journal of Advances and Current Practices in Mobility. 2021;3:1993-2008.

[113] Attard WP, Bassett M, Parsons P, Blaxill H. A new combustion system achieving high drive cycle fuel economy improvements in a modern vehicle powertrain. SAE Technical Paper 2011-01-0664; 2011.

[114] Allison P, de Oliveira M, Giusti A, Mastorakos E. Pre-chamber ignition mechanism: Experiments and simulations on turbulent jet flame structure. Fuel. 2018;230:274-81.

[115] Shapiro E, Ahmed I, Tiney N. Advanced ignition modelling for pre-chamber combustion in lean burn gas engines. Ignition Systems for Gasoline Engines: Internationale Tagung Zündsysteme für Ottomotoren. 2018:104.

[116] Iacovano C, d'Adamo A, Cantore G. Analysis and simulation of non-flamelet turbulent combustion in a research optical engine. Energy Procedia. 2018;148:463-70.

[117] Gholamisheeri M, Thelen B, Toulson E. CFD modeling and experimental analysis of a homogeneously charged turbulent jet ignition system in a rapid compression machine. SAE Technical Paper 2017-01-0557; 2017.

[118] Thelen BC, Gentz G, Toulson E. Computational study of a turbulent jet ignition system for lean burn operation in a rapid compression machine. SAE Technical Paper 2015-01-0396; 2015.

[119] Kariuki J, Dowlut A, Yuan R, Balachandran R, Mastorakos E. Heat release imaging in turbulent premixed methane–air flames close to blow-off. Proceedings of the Combustion Institute. 2015;35:1443-50.

[120] Ju D, Huang Z, Li X, Zhang T, Cai W. Comparison of open chamber and pre-chamber ignition of methane/air mixtures in a large bore constant volume chamber: Effect of excess air ratio and pre-mixed pressure. Applied Energy. 2020;260:114319.

[121] Schlatter S, Schneider B, Wright YM, Boulouchos K. Comparative study of ignition systems for lean burn gas engines in an optically accessible rapid compression expansion machine.

SAE Technical Paper 2013-24-0012; 2013.

[122] Gentz G, Thelen B, Gholamisheeri M, Litke P, Brown A, Hoke J, et al. A study of the influence of orifice diameter on a turbulent jet ignition system through combustion visualization and performance characterization in a rapid compression machine. Applied Thermal Engineering. 2015;81:399-411.

[123] Macián V, Salvador FJ, De la Morena J, Pagano V. Combustion analysis of a stratified pre-chamber ignition system by means of a zero-dimensional turbulence and flame speed model. Combustion and Flame. 2021;232:111526.

[124] Sementa P, Catapano F, Di Iorio S, Vaglieco BM. Experimental Investigation of a Fueled Prechamber Combustion in an Optical Small Displacement SI Methane Engine. SAE Technical Paper 2019-24-0170; 2019.

[125] Sampath R, Tang Q, Marquez ME, Sharma P, Hlaing P, Houidi MB, et al. Study on the pre-chamber fueling ratio effect on the main chamber combustion using simultaneous PLIF and OH* chemiluminescence imaging. SAE Technical Paper 2020-01-2024; 2020.

[126] Sadanandan R, Markus D, Schießl R, Maas U, Olofsson J, Seyfried H, et al. Detailed investigation of ignition by hot gas jets. Proceedings of the Combustion Institute. 2007;31:719-26.

[127] Russwurm T, Schumacher M, Wensing M. Active fuelling of a passenger car sized pre-chamber ignition system with gaseous components of gasoline. SAE Technical Paper 2020-01-2045; 2020.

[128] Schumacher M, Russwurm T, Wensing M. Pre-chamber ignition system for homogeneous lean combustion processes with active fuelling by volatile fuel components. Ignition Systems for Gasoline Engines: 4th International Conference, December 6-7, 2018, Berlin, Germany Ed: M Günther2018. p. 292.

[129] Mounaïm-Rousselle C, Landry L, Halter F, Foucher F. Experimental characteristics of turbulent premixed flame in a boosted Spark-Ignition engine. Proceedings of the Combustion Institute. 2013;34:2941-9.

[130] Bunce M, Peters N, Subramanyam SP, Blaxill H. Assessing the low load challenge for jet ignition engine operation. Internal Combustion Engines and Powertrain Systems for Future Transport, December 11-12, 2019, Birmingham, UK: CRC Press; 2020. p. 3.

[131] Taghavifar H, Jafarmadar S, Taghavifar H, Navid A. Application of DoE evaluation to introduce the optimum injection strategy-chamber geometry of diesel engine using surrogate epsilon-SVR. Applied Thermal Engineering. 2016;106:56-66.

[132] Moiz AA, Pal P, Probst D, Pei Y, Zhang Y, Som S, et al. A machine learning-genetic algorithm (ML-GA) approach for rapid optimization using high-performance computing. SAE International Journal of Commercial Vehicles. 2018;11:291-306.

[133] Cho S, Park J, Song C, Oh S, Lee S, Kim M, et al. Prediction modeling and analysis of knocking combustion using an improved 0D RGF model and supervised deep learning. Energies. 2019;12.

[134] Petrucci L, Ricci F, Mariani F, Cruccolini V, Violi M. Engine knock evaluation using a machine learning approach. SAE Technical Paper 2020-24-0005; 2020.

[135] Badra JA, Khaled F, Tang M, Pei Y, Kodavasal J, Pal P, et al. Engine combustion system optimization using computational fluid dynamics and machine learning: A methodological approach. Journal of Energy Resources Technology. 2020;143.

[136] Posch S, Winter H, Zelenka J, Pirker G, Wimmer A. Development of a tool for the

preliminary design of large engine prechambers using machine learning approaches. Applied Thermal Engineering. 2021;191:116774.